Conserved NDR/LATS kinase controls RAS GTPase activity to regulate cell growth and chronological lifespan

Chuan Chen, Marbelys Rodriguez Pino†, Patrick Roman Haller†, and Fulvia Verde*
Department of Molecular and Cellular Pharmacology, University of Miami Miller School of Medicine, Miami, FL 33136

ABSTRACT **Adaptation to the nutritional environment is critical for all cells. RAS GTPase is a highly conserved GTP-binding protein with crucial functions for cell growth and differentiation in response to environmental conditions. Here, we describe a novel mechanism connecting RAS GTPase to nutrient availability in fission yeast. We report that the conserved NDR/LATS kinase Orb6 responds to nutritional cues and regulates Ras1 GTPase activity. Orb6 increases the protein levels of an Ras1 GTPase activator, the guanine nucleotide exchange factor Efc25, by phosphorylating Sts5, a protein bound to *efc25* mRNA. By manipulating the extent of Orb6-mediated Sts5 assembly into RNP granules, we can modulate Efc25 protein levels, Ras1 GTPase activity, and, as a result, cell growth and cell survival. Thus, we conclude that the Orb6–Sts5–Ras1 regulatory axis plays a crucial role in promoting cell adaptation, balancing the opposing demands of promoting cell growth and extending chronological lifespan.**

Monitoring Editor
Daniel J. Lew
Duke University

Received: Mar 26, 2019
Revised: Jul 26, 2019
Accepted: Aug 2, 2019

INTRODUCTION

RAS GTPases are highly conserved GTP-binding proteins that have crucial functions for cell polarization, growth, and differentiation in eukaryotes. Ras GTPases activate a number of conserved signaling pathways that promote these functions, such as the MAP kinase cascade and the mTOR pathway (Simanshu *et al.*, 2017). In humans, inappropriate activation of RAS has a causal role in cancer, congenital malformations (Rauen, 2013; Tidyman and Rauen, 2016), and neurodevelopmental disorders (Jeyabalan and Clement, 2016; Mignot *et al.*, 2016). While RAS is one of the most intensively studied signaling proteins, there is still much to learn about additional signaling pathways that interact functionally with RAS proteins, and this knowledge may provide additional targeting opportunities.

Here, we describe a novel mechanism that regulates RAS GTPase in response to nutrient availability, using the fission yeast *Schizosaccharomyces pombe* as a model system. Fission yeast cells modulate cell shape and the pattern of polarized cell growth in response to nutritional conditions (Mitchison and Nurse, 1985). Using fission yeast, we previously reported that polarized cell growth is controlled by the NDR (Nuclear Dbf2-Related) kinase Orb6 (Verde *et al.*, 1995, 1998). NDR kinases belong to a conserved subfamily (NDR/LATS) of AGC kinases that regulate cell morphogenesis, growth and proliferation, mitosis, and development (Verde *et al.*, 1995, 1998; Zinn, 2004; Hergovich *et al.*, 2006; Hergovich, 2016; Das *et al.*, 2009; Swaffer *et al.*, 2018). Dysregulation of mammalian NDR kinases (NDR1/2) has been implicated in different types of cancer (Millward *et al.*, 1998; Hauschild *et al.*, 1999; Ross *et al.*, 2000; Adeyinka *et al.*, 2002; Cornils *et al.*, 2010; Sharif and Hergovich, 2018).

The fission yeast NDR kinase Orb6 promotes polarized cell growth, in part, by phosphorylation of mRNA-binding protein Sts5 (Toda *et al.*, 1996; Nuñez *et al.*, 2016). Sts5 is homologous to human DIS3L2 (Astuti *et al.*, 2012), which is implicated in Perlman syndrome and Wilm's tumor (Astuti *et al.*, 2012; Malecki *et al.*, 2013; Lv *et al.*, 2015; Robinson *et al.*, 2015); the molecular details of Sts5 regulation and its downstream effectors, however, have not been fully characterized. Upon Orb6 kinase inhibition or nutritional deprivation, Sts5 proteins assemble into cytoplasmic ribonucleoprotein particles (RNPs) that colocalize with processing bodies (P-bodies) (Nuñez *et al.*, 2016), which are sites of mRNA storage and degradation (Decker and Parker, 2012).

Coalescence of mRNA-binding proteins is a conserved, adaptive mechanism of response to stress (Riback *et al.*, 2017). In this study, we show that the conserved NDR kinase Orb6, an essential kinase that controls cell morphogenesis during exponential cell growth,

This article was published online ahead of print in MBoC in Press (http://www.molbiolcell.org/cgi/doi/10.1091/mbc.E19-03-0172) on August 7, 2019.

†These authors contributed equally to this work.

*Address correspondence to: Fulvia Verde (fverde@miami.edu).

Abbreviations used: CRIB, Cdc42/Rac interactive binding; GEF, guanine nucleotide exchange factor; GFP, green fluorescent protein; LATS, large tumor suppressor; NDR, nuclear Dbf2-related; RFP, red fluorescent protein; RNP, ribonucleoprotein particle; YFP, yellow fluorescent protein.

also regulates cell adaptation during nutrient deprivation and cell quiescence. By phosphorylating a specific site in the N-terminal intrinsically disordered region of the mRNA-binding protein Sts5, Orb6 kinase inhibits Sts5 RNP granule assembly and the degradation of Ras1 guanine nucleotide exchange factor (GEF) *efc25* mRNA, thereby promoting Ras1 GTPase activity. We show that down-regulation of the Orb6–Sts5–Ras1 regulatory axis has a crucial role in cell adaptation, promoting chronological lifespan extension and survival during cell quiescence. Thus, we conclude that the NDR/LATS kinase Orb6, by regulating the extent of Sts5 RNP assembly, plays a key role in balancing the opposing demands of promoting cell growth and extending cell lifespan.

RESULTS

Orb6 kinase activity and Ras1 GTPase activity decrease upon nitrogen starvation

In fission yeast, nitrogen starvation alters cell shape and promotes entry into mitosis at a smaller cell size (Nurse and Bissett, 1981; Su *et al.*, 1996). Removal of nitrogen from the growth medium leads rapidly to reduced bipolar calcofluor staining (Supplemental Figure S1, A–C), to a decreased tip localization of the secretory marker Bgs4-RFP (Supplemental Figure S1E), and to decreased cell length (Supplemental Figure S1, A and D). Moreover, both CRIB-GFP, a biomarker for active Cdc42 (Tatebe *et al.*, 2008), and Gef1-3YFP, a Cdc42 guanine nucleotide exchange factor, are mislocalized at the cell periphery during nitrogen starvation (Figure 1, A–C). These phenotypes resemble the morphological changes of cells following Orb6 kinase inhibition or decreased Orb6 kinase levels (Verde *et al.*, 1998; Das *et al.*, 2009; Tay *et al.*, 2019).

Thus, we asked whether the activity of Orb6 kinase responds to nitrogen deprivation. To analyze Orb6 activity, we developed a novel phosphospecific antibody against Gef1 Ser-112, which is the specific Orb6 phosphorylation site in the Orb6 substrate Gef1, a guanine nucleotide exchange factor for Cdc42 (Das *et al.*, 2015). We found that this phosphospecific antibody can readily recognize phosphorylated Ser-112 in Gef1 (hereafter written as pGef1), but not the mutant protein (Gef1S112A) where Ser-112 has been mutated to alanine (Supplemental Figure S2A). This antibody can also visualize the decreased level of Gef1S112 phosphorylation in analogue-sensitive *orb6-as2* mutant cells upon 1-NA-PP1 inhibitor treatment, as compared with that in *orb6-as2* mutant cells treated with DMSO (dimethyl sulfoxide) and in *orb6+* wild-type cells treated with either DMSO or 1-NA-PP1 (Supplemental Figure S2, B and C). We found that the pGef1 level decreases rapidly upon depletion of nitrogen from the growth medium, suggesting that Orb6 kinase activity decreases following nitrogen starvation (Figure 1, D and E).

We previously identified a set of mRNAs that bind to Sts5, including *efc25* (Nuñez *et al.*, 2016), encoding a GEF for Ras1 GTPase (Tratner *et al.*, 1997; Papadaki *et al.*, 2002). When Orb6 kinase activity is inhibited, Sts5 RNP granules are assembled, *efc25* translation is repressed, and Efc25 protein levels decrease (Nuñez *et al.*, 2016). Here, we find that Efc25 protein levels also decrease upon nitrogen depletion (Figure 1, F and G). This decrease in Efc25 protein level is partially suppressed by *sts5*Δ (Supplemental Figure S3, A and B). Loss of Sts5 increases Efc25 protein level in the absence of nitrogen starvation, indicating that Sts5 has an important function in the homeostasis of Efc25 protein levels (Nuñez *et al.*, 2016). However, *sts5*Δ also affects the overall shape of the nonlinear fit curve of Efc25 decay during nitrogen starvation (Supplemental Figure S3, A and C), indicating that Efc25 protein decrease is dependent, at least in part, on increased Sts5 RNP granule formation. Consistent with these findings, Sts5 RNP puncta assembly increases following nitrogen starvation (Figure 1, H and I), and the number of Sts5 RNP puncta correlates negatively with Efc25 protein levels (Supplemental Figure S3D).

Thus, we tested whether Ras1 GTPase activity decreases upon nitrogen starvation as the levels of Ras1 GEF Efc25 decrease. By using the biomarker RasAct-3GFP, which only binds to the active (GTP-bound) form of Ras1 GTPase (Merlini *et al.*, 2018), we observed that the intensity of the RasAct-3GFP signal at the cell tips rapidly decreases following nitrogen starvation (Figure 1, J, a–d, and K). No change in the protein level of the RasAct-3GFP biomarker was detected (Supplemental Figure S4, A and B) during the course of this experiment.

In fission yeast, Ras1 promotes polarized cell growth by recruiting Scd1, one of the guanine nucleotide exchange factors of Cdc42 GTPase, to the cell tips (Chang *et al.*, 1994; Tratner *et al.*, 1997; Papadaki *et al.*, 2002; Onken *et al.*, 2006). Tip localization of Scd1-3GFP is strongly decreased and less polarized in the *ras1*Δ background (Supplemental Figure S4, C and D), while the protein level of Scd1-3GFP is not affected (Supplemental Figure S4, E and F). Consistent with nitrogen starvation leading to reduced Ras1 activity, Scd1-3GFP intensity at the cell tips is significantly decreased following nitrogen starvation (Figure 1, J, e–h, and L). Scd1-3GFP protein levels decrease upon nitrogen starvation as well (Supplemental Figure S4, G and H), suggesting that Scd1 protein levels is also controlled by other nitrogen-responsive mechanisms, independent of Ras1.

We conclude that both Orb6 kinase activity and Ras1 GTPase activity decrease upon nitrogen starvation, and that the decrease in Ras1 GEF Efc25 protein levels is dependent, at least in part, upon increased Sts5 coalescence into granules.

Orb6 kinase promotes Ras1 GTPase activity in an Sts5-dependent manner

Next, we investigated whether Orb6 kinase controls Ras1 GTPase activity by using the biomarker RasAct-3GFP as described above (Merlini *et al.*, 2018). We observed that the intensity of the RasAct-3GFP signal decreases rapidly in analogue-sensitive *orb6-as2* mutant cells upon 1-NA-PP1 inhibitor treatment (Figure 2 Ad, arrows, and B), while no change was observed in *orb6-as2* mutant cells treated with DMSO (Figure 2, Ac and B), nor in *orb6+* wild-type cells treated with either DMSO or 1-NA-PP1 (Figure 2, A, a–b, and B). The time course of this experiment is shown in Supplemental Figure S5, A, a–c, and B. No change in the protein level of the RasAct-3GFP biomarker was detected (Supplemental Figure S5, D and E) during the course of this experiment. Consistent with the idea that Ras1 GTPase activity is, at least in part, negatively regulated by Sts5 mRNA binding protein, we found that the decrease in RasAct-3GFP tip intensity upon Orb6 inhibition is suppressed by the deletion of *sts5* (Figure 2, Dd, asterisks, and E).

Consistent with Orb6 inhibition leading to reduced Ras1 activity, Scd1-3GFP intensity at the cell tips is significantly decreased in analogue-sensitive *orb6-as2* cells treated with 1-NA-PP1 (Figure 2, Ah and C), as compared with *orb6-as2* cells treated with DMSO (Figure 2, Ag and C) or with *orb6+* wild-type cells treated with either DMSO or 1-NA-PP1 (Figure 2, A, e and f, and C). The time course of this experiment is shown in Supplemental Figure S5, A, d–f, and C. The protein level of Scd1-3GFP did not change during the course of this experiment (Supplemental Figure S5, F and G).

Thus, our results show that Ras1 GTPase is a downstream effector of the Orb6–Sts5 pathway and that Orb6 kinase promotes Ras1 GTPase activity in a Sts5-dependent manner.

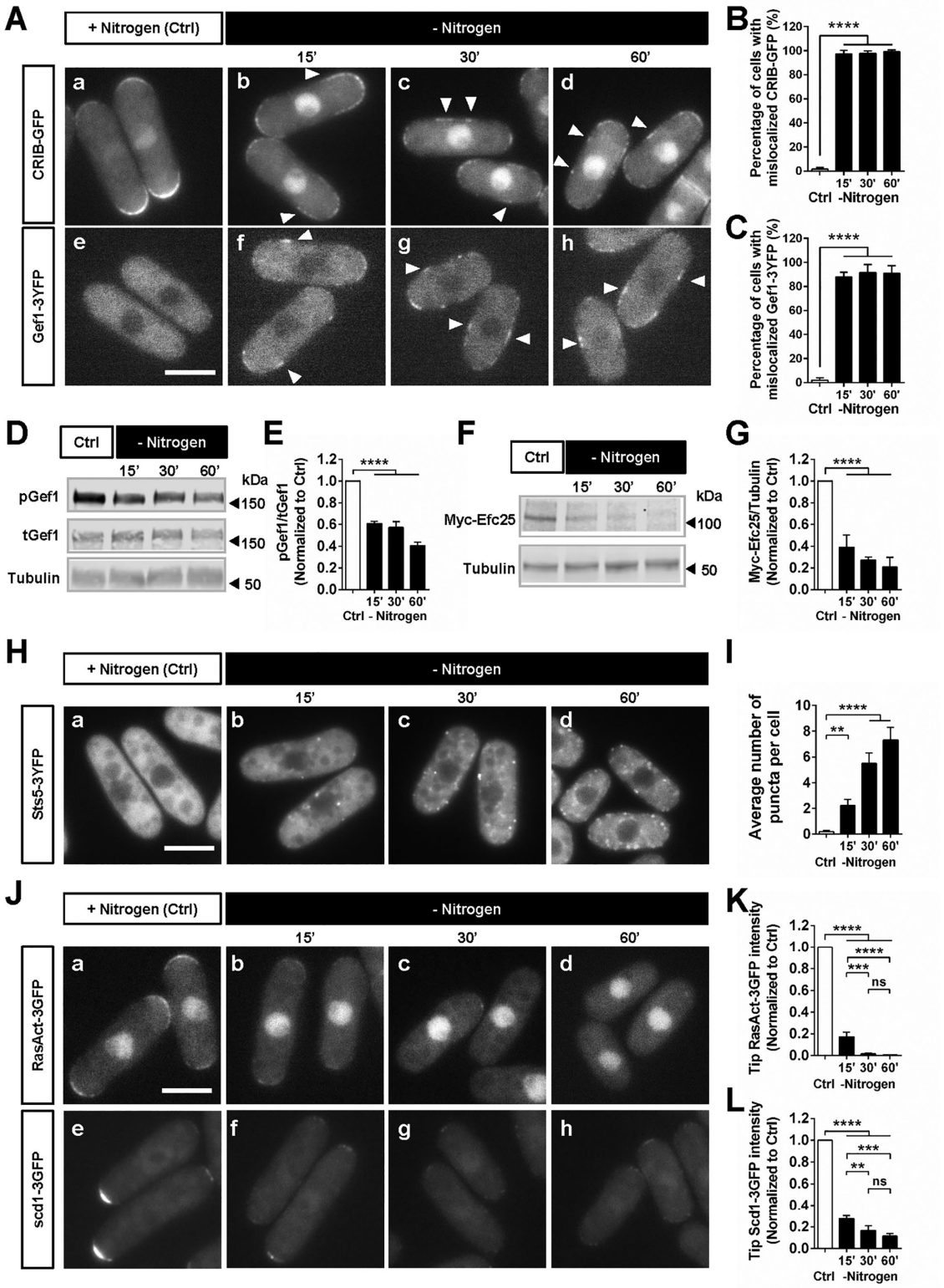

FIGURE 1: Orb6 kinase activity and Ras1 GTPase activity decrease under nitrogen starvation. (A) CRIB-GFP and Gef1-3YFP are mislocalized at cell sides following nitrogen starvation. *CRIB-GFP* and *gef1-3YFP* cells cultured in EMM+N were washed twice with EMM minus nitrogen and resuspended in EMM with (Ctrl) or without nitrogen. Images are deconvolved projections from six Z-stacks separated by a step size of 0.3 μm. Scale bar = 5 μm. (B, C) Quantification of the experiment shown in A based on three independent experiments. The percentage of cells with mislocalized CRIB-GFP or Gef1-3YFP is significantly increased after nitrogen deprivation following a time course (15, 30, and 60 min) compared with that in EMM+N controls. Data are presented as mean ± SD; *p* values are determined by one-way ANOVA followed by Dunnett's multiple comparison test. ****$p < 0.0001$. (D) Orb6 kinase activity decreases under nitrogen starvation. Western blotting using antibodies to visualize pGef1 and tGef1 was performed in *gef1-3YFP* cells

Orb6-mediated phosphorylation of the Sts5 N-terminal intrinsically disordered region controls RNP assembly and Ras1 activity

Our results show that in response to nitrogen starvation, Orb6 kinase activity is down-regulated, and that down-regulation of Orb6 kinase activity leads to decreased Ras1 GTPase activity, in a manner dependent on the mRNA-binding protein Sts5. We then addressed the molecular mechanisms underlying the Orb6–Sts5–Ras1 regulatory pathway. The Sts5 protein sequence includes an intrinsically disordered region (IDR) at the N-terminus (Nuñez *et al.*, 2016; Figure 3A). Recent studies indicated that intrinsically disordered protein domains mediate RNP granule assembly (Kurischko *et al.*, 2011; Molliex *et al.*, 2015). We asked whether the N-terminal IDR of Sts5 is sufficient for Sts5 granule assembly. We endogenously expressed *sts5Nterm* (amino acids 1–284; Figure 3A), tagged with 3YFP, and observed Sts5Nterm-3YFP localization upon glucose starvation, a condition that promotes the assembly of larger RNP granules, easily visualized (Nuñez *et al.*, 2016). We found that glucose starvation readily induces Sts5Nterm-3YFP assembly into cytoplasmic RNP puncta (Figure 3Bd), which colocalize with the P-bodies, as visualized by the P-body marker Dcp1-mCherry (Figure 3B, e and f). Conversely, Sts5Nterm-3YFP and Dcp1-mCherry proteins are diffusely localized in the cytoplasm under glucose-rich culture conditions (Figure 3B, a–c), as previously reported for the full-length Sts5 protein (Nuñez *et al.*, 2016). Thus, these findings indicate that the Sts5 disordered domain mediates Sts5 coalescence into RNP granules.

Further, we asked how Orb6 kinase regulates Sts5 coalescence into RNP granules. Previous studies of NDR/LATS kinases in other model systems, including *Saccharomyces cerevisiae* CBK1, mammalian NDR/LATS kinases, and *S. pombe* Orb6, identified Hx[R/K/H]xx[S/T] as phosphorylation consensus for these kinases (Hao *et al.*, 2008; Mazanka *et al.*, 2008; Swaffer *et al.*, 2018). We found that phosphorylation of the Orb6 targets Gef1 and Sts5 promotes their association with the 14-3-3 protein Rad24 (Das *et al.*, 2015; Nuñez *et al.*, 2016), which belongs to a class of highly conserved regulatory proteins (Yaffe *et al.*, 1997; Hermeking and Benzinger, 2006). Deletion of *rad24* leads to increased Sts5 RNP assembly, indicating a negative regulatory role of the 14-3-3 protein Rad24 in Sts5 RNP coalescence (Nuñez *et al.*, 2016). Intriguingly, the N-terminal domain of Sts5 contains a unique site that fits both the NDR/LATS phosphorylation consensus and the 14-3-3 binding motif (amino acids 81–86; HRRSAS*; Figure 3A, magenta arrow). Thus, we asked whether Orb6 phosphorylates Sts5 at Ser-86 to promote the association with the 14-3-3 protein Rad24. We engineered a nonphosphorylatable mutation at the Sts5 Ser-86 site (*sts5S86A*). By using an in vitro thiophosphorylation assay (*Materials and Methods*), we found that the immunopurified Orb6-as2 kinase (Wiley *et al.*, 2003; Das *et al.*, 2015; Nuñez *et al.*, 2016) directly phosphorylates bacterially expressed Sts5Nterm but not Sts5NtermS86A proteins (Supplemental Figure S6). Further, we tested for the association of full-length Sts5S86A protein with bacterially expressed 14-3-3 protein GST-Rad24 (Das *et al.*, 2015; Nuñez *et al.*, 2016). We found that Sts5S86A-HA displays a significantly decreased association with Rad24, as compared with the wild-type Sts5-HA protein (Figure 3, C and D). These results indicate that Orb6 kinase phosphorylates Sts5 at Ser-86 and thereby promotes Sts5 association with the 14-3-3 protein Rad24.

Next, we asked whether the *sts5S86A* mutant reproduces the Sts5-dependent Orb6 kinase inhibition effects. We found that Efc25 protein levels are significantly decreased in the *sts5S86A* mutant, compared with those in control *sts5+* cells (Figure 3, E and F; see the model in Figure 3I). Consistently, we found that RasAct-3GFP tip intensity increases in *sts5Δ* and decreases in *sts5S86A* mutant cells (Figure 3, G and H) in a manner that correlates with the increase or decrease in Efc25 protein levels (Figure 3, E and F).

Together, our results show that the molecular details of the Orb6–Sts5–Ras1 pathway involve two sequential negative interactions (Figure 3I): Orb6 inhibits mRNA-binding protein Sts5 coalescence into RNP granules by phosphorylating Sts5 at Ser-86 and promoting Sts5 association with the 14-3-3 protein Rad24. This mechanism prevents the translational repression of Sts5-associated

cultured in EMM plus NH_4Cl (nitrogen resource) (EMM+N) at 30°C. Cells were washed twice with EMM minus NH_4Cl (EMM-N) and resuspended in EMM with (Ctrl) or without nitrogen. Tubulin levels were determined as a loading control. (E) Quantification of pGef1/tGef1 normalized to the EMM+N group (Ctrl) depicted in D based on three independent experiments. The level of phosphorylated Gef1S112 is significantly decreased after nitrogen deprivation following a time course (15, 30, and 60 min). Data are presented as mean ± SD; *p* values are determined by one-way ANOVA followed by Dunnett's multiple comparison test. ****$p < 0.0001$. (F) Myc-Efc25 protein level decreases under nitrogen starvation. Western blotting using an anti-Myc antibody to visualize Myc-Efc25 was performed in *myc-efc25* cells cultured in EMM+N at 25°C. Cells were washed twice with EMM-N and resuspended in EMM with (Ctrl) or without nitrogen. Tubulin levels were determined as a loading control. (G) Quantification of Myc-Efc25/tubulin normalized to the EMM+N group (Ctrl) depicted in F based on three independent experiments. The level of Myc-Efc25/tubulin is significantly decreased after nitrogen deprivation following a time course (15, 30, and 60 min). Data are presented as mean ± SD; *p* values are determined by one-way ANOVA followed by Dunnett's multiple comparison test. ****$p < 0.0001$. (H) Sts5-3YFP cytoplasmic RNP puncta formation following nitrogen starvation. Images are deconvolved projections from six Z-stacks with a step size of 0.3 µm. Scale bar = 5 µm. (I) Quantification of Sts5-3YFP RNP puncta numbers per cell in the experiments depicted in H based on three independent experiments. The average number of puncta per cell was significantly increased following nitrogen starvation. Data are presented as mean ± SD; *p* values are determined by one-way ANOVA followed by Dunnett's multiple comparison test. **$p < 0.01$, ****$p < 0.0001$. (J) Tip intensity of RasAct-3GFP and Scd1-3GFP is decreased under nitrogen starvation. *RasAct-3GFP* and *scd1-3GFP* cells cultured in EMM+N were washed twice with EMM minus nitrogen and resuspended in EMM with (Ctrl) or without nitrogen. Images are deconvolved projections from six Z-stacks with a step size of 0.3 µm. Scale bar = 5 µm. (K, L) Quantification of the experiment shown in J based on three independent experiments. The total intensity of RasAct-3GFP (G, a–d) and Scd1-3GFP (G, e–h) is significantly decreased after nitrogen deprivation following a time course (15, 30, and 60 min) compared with that for EMM+N controls. Data are presented as mean ± SD; *p* values are determined by one-way ANOVA followed by Dunnett's multiple comparison test. **$p < 0.01$, ***$p < 0.001$, ****$p < 0.0001$. ns, not statistically significant.

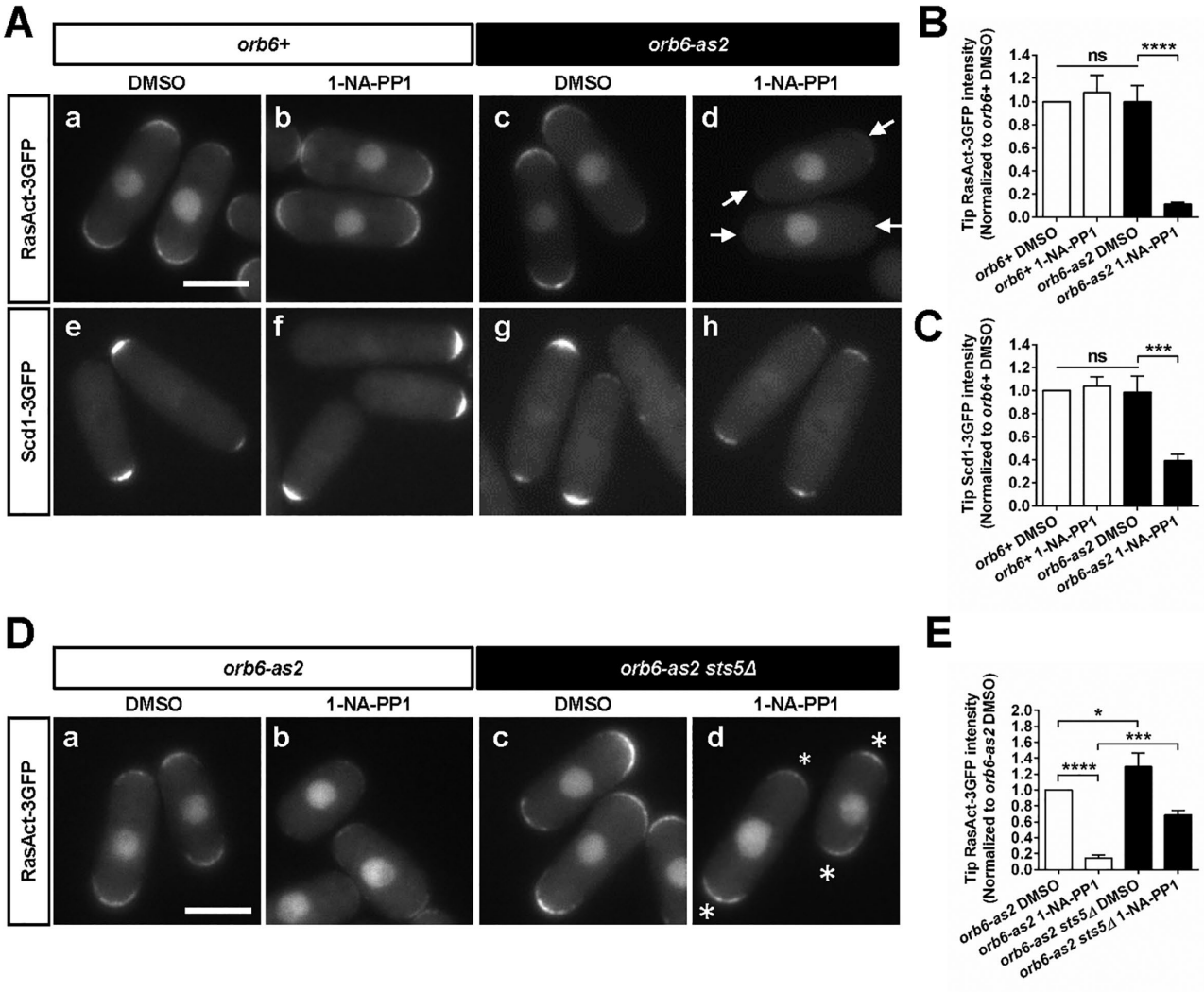

FIGURE 2: Orb6 kinase promotes Ras1 GTPase activity in a Sts5-dependent manner. (A) Tip intensity of RasAct-3GFP and Scd1-3GFP is decreased under Orb6 inhibition. *orb6+ RasAct-3GFP* (a and b) and *orb6-as2 RasAct-3GFP* (c and d) cells cultured in EMM medium at 30°C were treated with DMSO (a and c) or 1-NA-PP1 (b and d) for 30 min. *orb6+ scd1-3GFP* (e and f) and *orb6-as2 scd1-3GFP* (g and h) cells cultured in EMM at 30°C were treated with DMSO (e and g) or 1-NA-PP1 (f and h) for 30 min. Images are deconvolved projections from six Z-stacks separated by a step size of 0.3 µm. Scale bar = 5 µm. Arrows denote decrease in RasAct-3GFP intensity at cell tips in *orb6-as2* cells treated with 1-NA-PP1. (B) Quantification of the experiment shown in A (a–d) based on three independent experiments. The total RasAct-3GFP intensity at both tips per cell was quantified and compared. *orb6-as2 RasAct-3GFP* cells treated with 1-NA-PP1 for 30 min show significantly decreased total RasAct-3GFP intensity compared with *orb6-as2 RasAct-3GFP* cells treated with DMSO or *orb6+ RasAct-3GFP* cells treated with either DMSO or 1-NA-PP1. Data are presented as mean ± SD; *p* values are determined by one-way ANOVA followed by Dunnett's multiple comparison test. ****$p < 0.0001$. ns, not statistically significant. (C) Quantification of the experiment shown in A (e–h) based on three independent experiments. The total Scd1-3GFP intensity at both tips per cell was quantified and compared. *orb6-as2 scd1-3GFP* cells treated with 1-NA-PP1 for 30 min show significantly decreased total Scd1-3GFP intensity from *orb6-as2 scd1-3GFP* cells treated with DMSO or *orb6+ scd1-3GFP* cells treated with either DMSO or 1-NA-PP1. Data are presented as mean ± SD; *p* values are determined by one-way ANOVA followed by Dunnett's multiple comparison test. ***$p < 0.001$. ns, not statistically significant. (D) Decrease in tip RasAct-3GFP intensity upon Orb6 inhibition is suppressed by *sts5*Δ. *orb6-as2 RasAct-3GFP* cells and *orb6-as2 sts5*Δ *RasAct-3GFP* cells cultured in EMM at 30°C were treated with DMSO (a and c) or 1-NA-PP1 (b and d) for 30 min. Images are deconvolved projections from six Z-stacks with step size 0.3 µm. Scale bar = 5 µm. Asterisks denote minimized decrease in RasAct-3GFP intensity at cell tips in *sts5*Δ background. (E) Quantification of the experiment shown in D based on three independent experiments. The total RasAct-3GFP intensity at both tips per cell was quantified and compared. Under control (DMSO) conditions, *orb6-as2 sts5*Δ *RasAct-3GFP* cells exhibit significantly increased RasAct-3GFP tip intensity from *orb6-as2 RasAct-3GFP* cells. *orb6-as2 RasAct-3GFP* cells treated with 1-NA-PP1 show significantly decreased tip RasAct-3GFP intensity from *orb6-as2 RasAct-3GFP* cells treated with DMSO. *orb6-as2 sts5*Δ *RasAct-3GFP* cells treated with 1-NA-PP1 show significantly increased total RasAct-3GFP intensity from *orb6-as2 RasAct-3GFP* cells treated with 1-NA-PP1. Data are presented as mean ± SD; *p* values are determined by one-way ANOVA followed by Dunnett's multiple comparison test. *$p < 0.05$, ***$p < 0.001$, ****$p < 0.0001$.

mRNAs, including Ras1 GEF mRNA *efc25*, thereby promoting RAS GTPase Ras1 activity.

Orb6 kinase reversibly modulates Ras1 activity and polarized cell growth during nitrogen starvation and recovery

Because our results indicate that down-regulation of Orb6 kinase activity leads to decreased Ras1 activity, and that Orb6 kinase activity decreases in response to nitrogen starvation, we tested whether a constitutively active Orb6 kinase suppresses the cellular response to nitrogen starvation. We engineered a constitutively active Orb6 kinase mutant (Orb6T456D), where aspartic acid replaces a phosphorylated threonine (T456) that promotes activity in this class of kinases (Stegert *et al.*, 2005). We integrated the construct using the Rep6x plasmid into the genome in single copy under the control of the *nmt1* promoter. We found that cells expressing *orb6T456D* display increased Orb6 kinase activity, as evidenced by higher pGef1 level in comparison with integrated *Rep6x* control (Supplemental Figure S7, A and B, lanes 1 and 3) and by decreased Sts5 granule formation upon nitrogen starvation in comparison with control (Supplemental Figure S7, Cd and D). Integrating a copy of the wild-type Orb6 protein also increased the readout pGef1 level, but not in a statistically significant manner (Supplemental Figure S7, A and B, lanes 1 and 2).

We found that *orb6T456D* mutant cells display higher RasAct-3GFP intensity at the cell tips under nitrogen-rich conditions (Figure 4, Ae, asterisks, and B) more than control cells (Figure 4, Aa and B). Furthermore, in *orb6T456D* mutant cells, the distribution of RasAct-3GFP is more symmetrically partitioned between old and new tips (Supplemental Figure S7E) and the pattern of cell growth is more bipolar (Supplemental Figure S7F). These findings suggest that a constitutively active Orb6 kinase promotes Ras1 GTPase activity and bipolar cell growth above the normal levels observed in wild-type cells. Consistent with Sts5 mediating these effects, *orb6T456D sts5S86A* double-mutant cells display decreased RasAct-3GFP tip intensity under nitrogen-rich conditions (Figure 4, Ai and B), decreased bipolar distribution of RasAct-3GFP, and decreased bipolar cell growth as compared with the *Rep6x* control or *orb6T456D* mutant cells (Supplemental Figure S7, E and F).

Then we tested how *orb6T456D* mutant cells respond to nitrogen starvation. We found that, following nitrogen removal, the decrease in Ras1 GTPase activity at the cell tips of *orb6T456D* mutant cells is significantly delayed (Figure 4, A, f–h, and C) as compared with control cells (Figure 4, A, b–d, and C). The promotion of Ras1 GTPase activity by the *orb6T456D* mutant is dependent on *sts5*, as evidenced by the accelerated decrease in Ras1 GTPase activity at the cell tips of the *orb6T456D sts5S86A* double mutant cells (Figure 4, A, j–l, and C).

Next, we tested whether Orb6 kinase also modulates the recovery of cells upon nitrogen refeeding following prolonged nitrogen starvation. We found that *orb6T456D* mutant cells display significantly faster recovery of RasAct-3GFP tip localization after nitrogen refeeding (Figure 4, D, f–h, and E) in comparison with control cells (Figure 4, D, b–d, and E). The rate of cell extension, as a measure of polarized cell growth, is also significantly increased in the *orb6T456D* mutant cells during recovery (Figure 4F and Supplemental Figure S8A).

Conversely, recovery is significantly delayed in *sts5S86A* cells as compared with control *sts5+* cells (Supplemental Figure S8, B–E). Consistent with Sts5 mediating the effects of Orb6 kinase, *orb6T456D sts5S86A* double-mutant cells display a significantly slower recovery of RasAct-3GFP tip localization after nitrogen refeeding (Figure 4, D, j–l, and E), and a decreased rate of cell extension (Figure 4F) in comparison with *orb6T456D* mutant cells.

Combined, these observations show that Orb6 kinase, by phosphorylating Sts5 at Ser-86, reversibly regulates Ras1 GTPase activity and cell growth, indicating a crucial role of the Orb6–Sts5–Ras1 axis in the cell response to nitrogen availability.

The "constitutively coalesced" Sts5S86A mutant protein enhances morphological adaptation during entry into quiescence

Next, we studied the role of the Orb6–Sts5–Ras1 pathway in regulating cell adaptation during entry into quiescence induced by high cell density. High cell density leads to physiological stress due to depletion of a variety of nutrients, including glucose and nitrogen (Yanagida, 2009; Yanagida *et al.*, 2011). We can experimentally monitor this type of nutrient depletion by following a cell culture growing to progressively higher cell densities (Nuñez *et al.*, 2016). The well-defined pattern of cell growth in *S. pombe* cells (Mitchison and Nurse, 1985) responds to nutrient availability in the environment, with cells becoming less bipolar upon nutritional stress (Su *et al.*, 1996; Yanagida, 2009; Yanagida *et al.*, 2011).

Thus, we then investigated the effect of *sts5S86A* mutation on growth pattern as cells grew to progressively higher cell densities. We found that under these growing conditions as well, the *sts5S86A* mutant cells display a decreased percentage of bipolar cells, as compared with the control *sts5+* cells, both under exponential growth (optical density at 600 nm < 0.4) and under nutrient depletion (optical density at 600 nm ≥ 0.4; Figure 5, A and B). Further, we found that *sts5S86A-3YFP* mutant cells display an increased number of Sts5 cytoplasmic RNP puncta, as compared with the control *sts5-3YFP* cells, both under exponential growth and under nutrient depletion (Figure 5, D and E). These findings suggest that the *sts5S86A* mutant cells display the "constitutively coalesced" phenotype, promoting Sts5 cytoplasmic RNP puncta assembly and morphological adaptation in response to nutrient depletion. Consistent with Sts5 assembly into RNP particles negatively controlling bipolar growth, the number of Sts5 RNP puncta and the percentage of bipolar cells display a strong negative correlation in both control *sts5* ($r = -0.8894$, $p < 0.001$) and mutant *sts5S86A* ($r = -0.8478$, $p < 0.001$) cells, with similar best fitting regression lines (Figure 5F).

Another distinct trait of *S. pombe* cells in response to nutrient depletion is entering mitosis at a decreased cell length (Costello *et al.*, 1986; Su *et al.*, 1996; Yanagida, 2009; Yanagida *et al.*, 2011). Here, we found that the *sts5S86A* mutant cells maintain a consistently shorter cell length at division than the control *sts5+* cells under both exponential and depleted growth conditions (Figure 5, A and C). Conversely, cell width is comparable in *sts5+*, *sts5Δ*, and *sts5S86A* cells (Supplemental Figure S9).

Overall, these results show that Orb6-mediated phosphorylation of Sts5 at Ser-86 is a key control mechanism for Sts5 cytoplasmic RNP puncta assembly, regulating the pattern of cell growth during exponential cell proliferation, and morphological adaptation during nutrient depletion.

Down-regulation of the Orb6–Sts5–Ras1 pathway promotes cell survival and extends lifespan during cell quiescence

We then investigated the physiological significance of the Orb6-Sts5-Ras1 pathway in regulating cell adaptation and survival in quiescence. Cells in stationary phase due to high cell density display a smaller size (Figure 6Ah) than cells growing exponentially in rich media (Figure 6Ad). Quiescent cells also show the assembly of Sts5 cytoplasmic granules colocalizing with the P-body marker

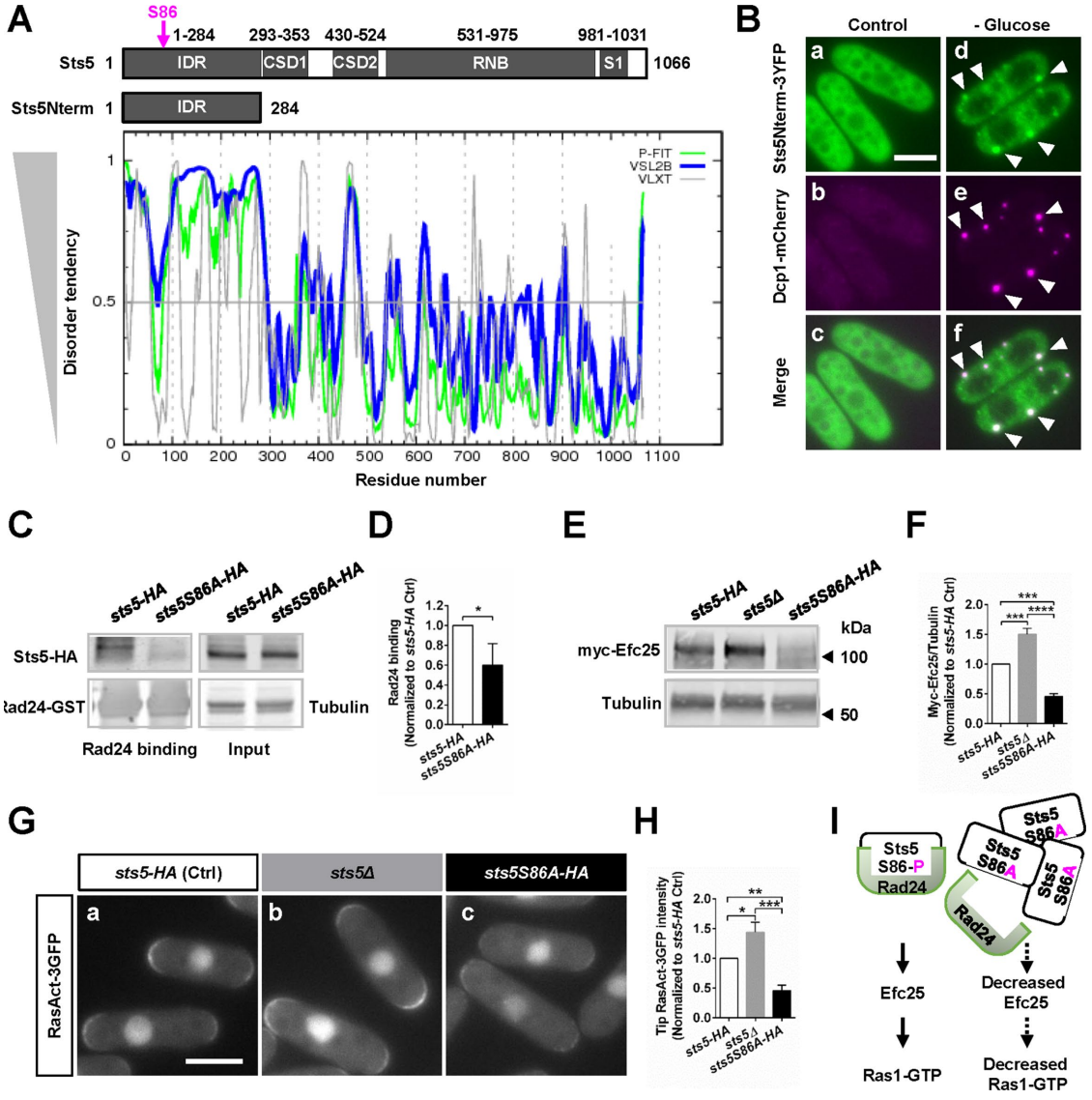

FIGURE 3: Orb6-mediated phosphorylation of Sts5 N-terminal intrinsically disordered region (IDR) controls RNP assembly and Ras1 activity. (A) Ser-86 (magenta arrow) of Sts5 protein is a putative Orb6/NDR phosphorylation site, which is also consistent with the 14-3-3 binding site upon phosphorylation. Ser-86 is predicted to be within the N-terminus intrinsically disordered region (IDR) by the Database of Protein Disorder (DisProt) using multiple algorithms including PONDR-FIT, VSL2B, and VLXT. The N-terminal IDR *sts5Nterm* (amino acids 1–284) tagged with 3YFP was cloned and integrated into the *sts5*Δ background under the endogenous promoter. (B) Sts5Nterm-3YFP is sufficient for Sts5 RNP granule assembly. *sts5Nterm-3YFP dcp-mCherry* cells cultured in the EMM at 30°C were washed twice with EMM minus glucose and resuspended in EMM with or without 2% glucose for 1 h. The truncated Sts5Nterm-3YFP protein and the P-body marker Dcp1-mCherry are diffusely localized in the cytoplasm in EMM with 2% glucose (a–c), while Sts5Nterm-3YFP protein forms cytoplasmic puncta upon glucose starvation, and the puncta are colocalized with the P-body marker Dcp1-mCherry (d–f). Puncta formation of Sts5Nterm-3YFP was observed as early as 15 min after transfer to glucose-depleted medium. Images are deconvolved projections from six Z-stacks separated by a step size of 0.3 µm. Scale bar = 5 µm. Arrowheads denote cytoplasmic RNP puncta. (C) 14-3-3 protein Rad24 binding is decreased in *sts5S86A* mutants. Physical association between endogenously expressed Sts5-HA or Sts5S86A-HA and bacterially expressed GST-Rad24 was detected using an anti-HA antibody after pulling down the GST-Rad24. Input of Sts5-HA or Sts5S86A-HA protein before the pull down was used as a loading control. (D) Quantification of pull-down experiment depicted in C based on three independent experiments. A significant reduction in the physical interaction between endogenously expressed Sts5S86A-HA and bacterially expressed GST-Rad24 was observed from the Sts5-HA. Data are presented as mean ± SD; *p* values are determined by two-tailed Student's *t* test. **p* < 0.05. (E) Myc-Efc25 protein level is increased in *sts5*Δ and decreased in *sts5S86A* mutants. Western blotting using an anti-Myc antibody to visualize Myc-Efc25 was performed in *sts5-HA* (control), *sts5*Δ, and *sts5S86A-HA* cells cultured in YE medium at 25°C. Tubulin levels were determined as a loading control. (F) Quantification of the experiment shown in E based on three independent experiments. Compared to *sts5-HA* control, Myc-Efc25/tubulin level is significantly increased in *sts5*Δ cells and is significantly decreased in *sts5S86A-HA* mutants. Data are presented as mean ± SD; *p* values are determined by one-way ANOVA followed by Dunnett's multiple comparison test. ****p* < 0.001, *****p* < 0.0001. (G) Tip intensity of

Dcp1-mCherry (Figure 6A, e–g), while exponentially growing cells do not (Figure 6A, a–c). Consistent with these findings, we found that in quiescence, Orb6 kinase activity is significantly lower (Figure 6, B and C), as assessed by analysis of pGef1 levels, similarly to what is found during nitrogen deprivation. Furthermore, we found that the Efc25 levels are significantly decreased when cells are in a stationary phase as compared with cells growing exponentially (Figure 6, D and E).

Thus, we asked whether Orb6 down-regulation during nutrient depletion promotes cell adaptiveness and robustness. We used the well-established colony forming–unit assay to evaluate lifespan of fission yeast, a measure of cell viability following nutritional depletion (Fabrizio and Longo, 2003; Roux *et al.*, 2006; Ocampo and Barrientos, 2011; Huang *et al.*, 2015). Cells are cultured to high densities in yeast extract (YE) medium. Considering that the pharmacokinetics and pharmacodynamics of the kinase inhibitor 1-NA-PP1 in prolonged culture are less well controlled, down-regulation of Orb6 kinase in these experiments is achieved by culturing *orb6-as2* mutant cells in YE medium that contains thiamine. The *orb6-as2* gene is placed under the control of the thiamine-responsive *nmt1* promoter, which is inactivated by the presence of thiamine (Das *et al.*, 2009). pGef1 levels significantly decrease when *orb6-as2* cells are cultured in YE medium, as compared with pGef1 level in wild-type cells cultured under the same condition (Supplemental Figure S10, A and B; *Materials and Methods*).

Remarkably, we found that the *orb6-as2* mutant cells are substantially more adaptive to nutritional stress, displaying a significantly longer lifespan in quiescence (Figure 6F, green line) compared with the control wild-type (*wt972*) cells (Figure 6F, black line). Consistent with a role for Sts5-mediated RNP assembly in promoting cell adaptiveness, we found that the *sts5*Δ mutant cells, which are defective in Sts5 RNP coalescence, display significantly decreased viability during cell quiescence and decreased lifespans (Figure 6F, magenta line) as compared with control cells. Supporting the idea that Sts5 mediates, at least in part, the adaptation phenotype observed in *orb6-as2* mutant cells, *orb6-as2 sts5*Δ double mutant cells display a shortened lifespan (Figure 6F, purple line) compared with *orb6-as2* cells. These results indicate that down-regulation of Orb6 kinase during nutrient depletion promotes cell adaptiveness and increases lifespan in a manner that is partially *sts5*-dependent.

Next, we investigated the effects of the *sts5S86A* and *orb6T456D* mutations on lifespan. We found that cells expressing the "constitutively coalesced" Sts5S86A mutant protein exhibit increased viability during nutrient depletion (Figure 6G, green line) compared with control cells (Figure 6G, black line). Conversely, constitutively active *orb6T456D* mutants display decreased cell viability (Figure 6G, magenta line). Consistent with Sts5 mediating the effect of Orb6 kinase, *sts5S86A* mutant partially suppresses the decreased viability of *orb6T456D* (Figure 6G, purple line).

Finally, we investigated the role of Efc25 and Ras1 in lifespan. We found that *efc25*Δ cells, which have decreased Ras1 activity (Merlini *et al.*, 2018), exhibit increased cell viability during nutrient depletion (Figure 6H, green line) in comparison with control (Figure 6H, black line). Intriguingly, it is the decrease in Efc25-mediated Ras1 activity, rather than in Ras1 protein per se, that promotes cell survival, since *ras1*Δ cells do not exhibit increased viability during nutrient depletion (Figure 6H, purple line) in comparison with the controls. Consistent with a role for Ras1 down-regulation in promoting cell survival in quiescence, the constitutively active Ras1 mutant *ras1G17V* exhibits decreased lifespan (Figure 6H, magenta line). Consistent with these findings, constitutively active Ras1 mutant *ras1G17V* partially suppresses the longevity phenotype of *orb6-as2* mutant (Figure 6I, purple line vs. green line).

These observations uncover a role for the Orb6–Sts5–Ras1 regulatory axis in the control of lifespan during cell quiescence. We find that modulating the extent of Sts5 assembly into RNP granules, mediated by Orb6 kinase activity, has a crucial role in increasing or decreasing cell adaptiveness and robustness during nutrient deprivation.

DISCUSSION

Orb6 kinase modulates Sts5 RNP granule assembly to control RAS GTPase activity

Cell growth control is a fundamental question in cell biology. Conserved regulatory pathways in nutrient sensing and growth control have important implications for human disease. One well-known example is the RAS pathway (Simanshu *et al.*, 2017), which has a fundamental role in controlling cell fate decisions, such as promoting cell proliferation or differentiation (Rauch *et al.*, 2016). The intricate web of regulatory interactions that control RAS activity is still not fully characterized.

Fission yeast has a single Ras protein, Ras1, and two guanine nucleotide exchange factors (GEFs), Efc25 and Ste6, that promote Ras1 activity and mediate distinct cellular functions (Papadaki *et al.*, 2002). On one hand, the constitutively expressed Efc25-mediated Ras1 pathway promotes cell polarization during mitotic growth (Papadaki *et al.*, 2002) by recruitment of Scd1, a guanine nucleotide exchange factor for the key polarity regulator GTPase Cdc42. In this manner, Ras1 initiates a GTPase cascade that promotes cell polarization (Chang *et al.*, 1994) during exponential cell growth. On the other hand, the pheromone-induced Ste6-mediated Ras1 pathway, functionally homologous to the mammalian RAS–RAF–MEK–ERK mitogenic pathway (Hughes *et al.*, 1993), promotes cell signaling required for mating (Hughes *et al.*, 1994; Merlini *et al.*, 2018).

RasAct-3GFP is increased in *sts5*Δ and decreased in *sts5S86A* mutants. *sts5-HA* control, *sts5*Δ, and *sts5S86A-HA* cells expressing the biomarker RasAct-3GFP were grown in EMM at 30°C. Images are deconvolved projections from six Z-stacks with step size 0.3 µm. Scale bar = 5 µm. (H) Quantification of the tip RasAct-3GFP intensity depicted in G based on three independent experiments. Compared with the *sts5-HA* control, the *sts5*Δ cells display a significantly increased RasAct-3GFP tip intensity, while the *sts5S86A-HA* mutants show a significantly decreased RasAct-3GFP tip intensity. Data are presented as mean ± SD; *p* values are determined by one-way ANOVA followed by Dunnett's multiple comparison test. *$p < 0.05$, **$p < 0.01$, ***$p < 0.001$. (I) Model recapitulating the effect of *sts5S86A* mutation on Sts5 puncta formation and Ras1 activity at cell tips. Wild-type Sts5 protein (left panel) is readily phosphorylated by Orb6 kinase on Ser-86 and binds to 14-3-3 protein Rad24. efc25 mRNA is actively translated into Efc25 protein, which promotes Ras1 activity at the cell tips. In contrast, the nonphosphorylatable mutant Sts5S86A protein (right panel) is predisposed to the assembly of RNP granules, where efc25 translation is repressed. Decreased level of Efc25 protein leads to decreased Ras1 activity at cell tips.

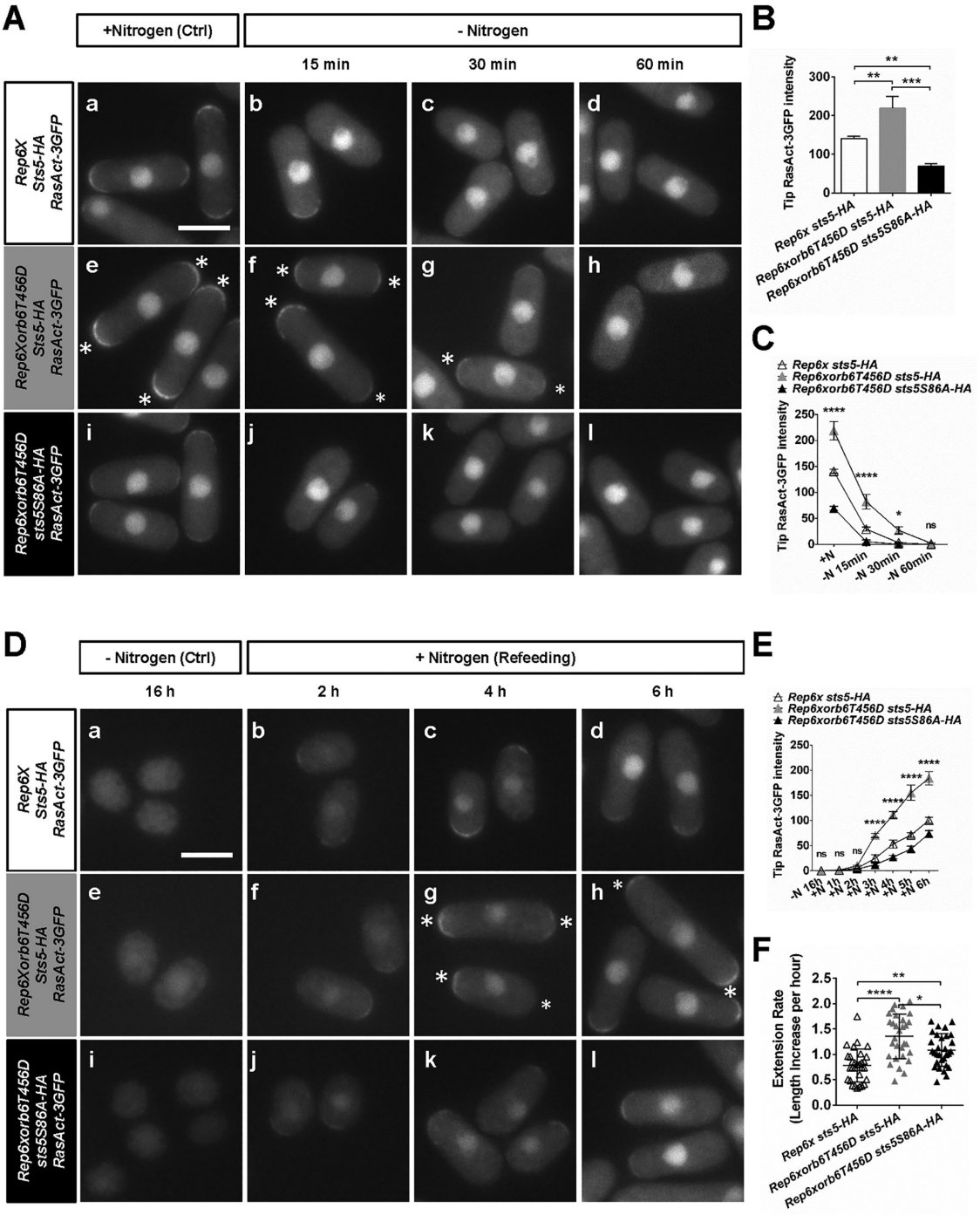

FIGURE 4: Orb6 kinase reversibly modulates Ras1 activity and polarized cell growth during nitrogen starvation and recovery. (A) Overexpression of constitutively active Orb6 kinase delays the decrease in Ras1 activity at cell tips following nitrogen starvation. *Rep6x sts5-HA RasAct-3GFP* (Ctrl), *Rep6xorb6T456D sts5-HA RasAct-3GFP*, and *Rep6xorb6T456D sts5S86A-HA RasAct-3GFP* cells cultured in EMM+N at 30°C were washed twice with EMM-N and resuspended in EMM with (Ctrl) or without nitrogen. Images were taken 15, 30, and 60 min after nitrogen starvation. Asterisks denote higher RasAct-3GFP intensity under EMM+N (Ctrl) conditions (e) and a delayed decrease under nitrogen starvation (f and g) in *Rep6xorb6T456D sts5-HA RasAct-3GFP* compared with *Rep6x sts5-HA RasAct-3GFP* (Ctrl). Cells in EMM+N were used as the control experiment. Scale bar = 5 μm. (B) Quantification of tip RasAct-3GFP intensity under control condition (EMM+N) depicted in A based on three independent experiments. In comparison with *Rep6x sts5-HA RasAct-3GFP* (Ctrl), *Rep6xorb6T456D sts5-HA RasAct-3GFP* cells have significantly increased RasAct-3GFP intensity at cell tips. *Rep6xorb6T456D sts5S86A-HA RasAct-3GFP* cells have significantly decreased RasAct-3GFP intensity at cell tips compared with both the control and the *Rep6xorb6T456D sts5-HA RasAct-3GFP* cells. Data are presented as mean ± SD; *p* values are determined by one-way ANOVA followed by Dunnett's multiple comparison test. $^{**}p < 0.01$, $^{***}p < 0.001$. (C) The tip RasAct-3GFP intensity was quantified and compared between groups after nitrogen starvation depicted in A based on three independent experiments. The tip RasAct-3GFP intensity of all groups was

Here, we report that Ras1 GTPase is a crucial downstream effector of the conserved NDR/LATS kinase Orb6 to balance the regulatory control of polarized cell growth and lifespan in response to nutritional availability. We find that Ras1 activity at the cell membrane depends on Orb6 kinase activity. Orb6 kinase promotes polarized cell growth, at least in part, through a positive regulatory pathway involving two sequential negative interactions: Orb6 inhibits mRNA-binding protein Sts5 association into RNP granules, thereby preventing the translational repression of Sts5-associated mRNAs. This simple but effective molecular mechanism promotes the translation of a number of morphology control factors, including the Ras1 guanine nucleotide exchange factor (GEF), Efc25.

By using mutant fission yeast strains (see the model in Figure 7), we demonstrate that the extent of assembly of mRNA binding protein Sts5 into RNP granules determines the activity levels of Ras1 GTPase by controlling the protein levels of Efc25. Recent studies have shown how cytoplasmic RNP granules are assembled by phase separation of intrinsically disordered proteins (Brangwynne *et al.*, 2009; Brangwynne, 2013; Lee *et al.*, 2013; Hyman *et al.*, 2014; Becker and Gitler, 2015; Elbaum-Garfinkle *et al.*, 2015; Kroschwald *et al.*, 2015; Lin *et al.*, 2015; Riback *et al.*, 2017). Phase separation can be regulated by phosphorylation, its effect depending on protein structure and electrostatic interactions between peptide sequences (Aumiller and Keating, 2016; Ambadipudi *et al.*, 2017; Larson *et al.*, 2017; Monahan *et al.*, 2017). We previously reported that Orb6 kinase, by promoting the interaction of Sts5 with the 14-3-3 protein Rad24, negatively regulates Sts5 assembly into RNP granules (Nuñez *et al.*, 2016). Here, we show that phosphorylation of a single amino acid in the disordered N-terminus of Sts5 (Ser-86) decreases Sts5 RNP granule assembly, thus increasing Efc25 protein levels and Ras1 activity. It should be noted that, because Sts5 has an important role in the control of Efc25 protein levels even during normal cell growth, Orb6 kinase may regulate other aspects of Sts5 function, irrespective of Sts5 RNP granule assembly. Indeed, there are two additional putative NDR/Orb6 phosphorylation sites in the RNB domain of Sts5, amino acids 633–638 HIRPTS* and amino acids 969–974 HIKIFS*. It is possible that Orb6 kinase also has a role in directly regulating Sts5 activity through these sites.

To our knowledge, this is the first time that NDR/LATS kinase has been shown to control RAS GTPase. Remarkably, this regulatory mechanism is mediated by RNP granule assembly, a dynamic and reversible biological process. Cytoplasmic RNP assembly is an adaptive mechanism for growth control and cell survival (Kroschwald and Alberti, 2017; Riback *et al.*, 2017; Franzmann and Alberti, 2019). Our results identify a novel biological mechanism that tethers Ras1 activity to mRNA metabolism in the cell.

Orb6 kinase activity controls polarized cell growth in response to nutritional availability

Fission yeast cells change cell morphology, becoming shorter and more monopolar, following nitrogen or glucose starvation (Fantes and Nurse, 1977; Perez-Hidalgo and Moreno, 2016). Mechanisms of this change in morphology are still unclear, although Cdc42 GTPase, a key morphology control factor in eukaryotes, appears to play an important role (Mutavchiev *et al.*, 2016).

In this study, we demonstrate for the first time that NDR kinase activity decreases during nutritional stress. Orb6 kinase activity decreases rapidly, within 15 min of nutritional stress onset, leading to a decrease in Ras1 GTPase activity and in the percentage of bipolar cells. Our current and previous observations indicate that Orb6 kinase controls polarized cell growth via multiple mechanisms. We have shown that loss of Orb6 activity leads to ectopic activation of Cdc42 GTPase at the membrane (Das *et al.*, 2009). Cdc42 GTPase is regulated by two GEFs, Scd1 and Gef1, with overlapping yet distinct functions: Scd1 is important for symmetry breaking, with loss of Scd1 leading to cells changing to a round shape (Chang *et al.*, 1994; Chiou *et al.*, 2017); conversely, Gef1 increases Cdc42 activity at the membrane (Coll *et al.*, 2003; Das *et al.*, 2012) and enlarges cell diameter (Das *et al.*, 2015). Previously we have shown that Orb6 kinase down-regulates the level of Gef1 at cell membrane by direct phosphorylation (Das *et al.*, 2015). Here, we show that Orb6 kinase increases the levels of Scd1 at cell tips by promoting the activity of Ras1, via regulation of Sts5. Thus, our results suggest that Orb6 kinase, by modulating the cortical levels of both Cdc42 GEFs, regulates the balance between Scd1 and Gef1, altering the pattern of cell growth in response to nutritional availability. Changes in the

decreased after nitrogen starvation. *Rep6xorb6T456D sts5-HA RasAct-3GFP* cells exhibit a delayed decrease in tip RasAct-3GFP intensity compared with the *Rep6x sts5-HA RasAct-3GFP* control cells. *Rep6xorb6T456D sts5S86A-HA RasAct-3GFP* cells exhibit an accelerated decrease in tip RasAct-3GFP intensity compared with the *Rep6xorb6T456D sts5-HA RasAct-3GFP* cells. Data are presented as mean ± SD; *p* values are determined by one-way ANOVA followed by Dunnett's multiple comparison test. *$p < 0.05$, ****$p < 0.0001$. ns, not statistically significant. (D) Overexpression of constitutively active Orb6 kinase promotes cell repolarization following nitrogen refeeding. *Rep6x sts5-HA RasAct-3GFP* (Ctrl), *Rep6xorb6T456D sts5-HA RasAct-3GFP*, and *Rep6xorb6T456D sts5S86A-HA RasAct-3GFP* cells cultured in EMM+N at 30°C were washed twice with EMM-N and resuspended in EMM-N for 16 h. Then the cells were refed with nitrogen by culture in EMM+N for up to 6 h. Images were taken at 16 h after nitrogen starvation and every 1 h after nitrogen refeeding. Cells after 16 h culture in EMM-N were used as the control experiment. Scale bar = 5 μm. (E) The tip RasAct-3GFP intensity was quantified and compared between groups after nitrogen starvation and refeeding in the experiments depicted in D based on three independent experiments. The tip RasAct-3GFP intensity of all groups increased after nitrogen refeeding. *Rep6xorb6T456D sts5-HA RasAct-3GFP* cells recovered tip RasAct-3GFP intensity faster and to a higher level than the *Rep6x sts5-HA RasAct-3GFP* control cells. *Rep6xorb6T456D sts5S86A-HA RasAct-3GFP* cells exhibit delayed recovery of tip RasAct-3GFP intensity compared with the *Rep6xorb6T456D sts5-HA RasAct-3GFP* cells. Data are presented as mean ± SD; *p* values are determined by one-way ANOVA followed by Dunnett's multiple comparison test at each time point. ****$p < 0.0001$. ns, not statistically significant. (F) Cell extension rate was quantified and compared between groups after nitrogen starvation and refeeding in the experiments depicted in D based on three independent experiments. *Rep6xorb6T456D sts5-HA RasAct-3GFP* cells exhibit an increased extension rate compared with *Rep6x sts5-HA RasAct-3GFP* control cells. *Rep6xorb6T456D sts5S86A-HA RasAct-3GFP* cells exhibit a decreased extension rate compared with the *Rep6xorb6T456D sts5-HA RasAct-3GFP* cells. Data are presented as mean ± SD; *p* values are determined by one-way ANOVA followed by Dunnett's multiple comparison test. *$p < 0.05$, **$p < 0.01$, ****$p < 0.0001$.

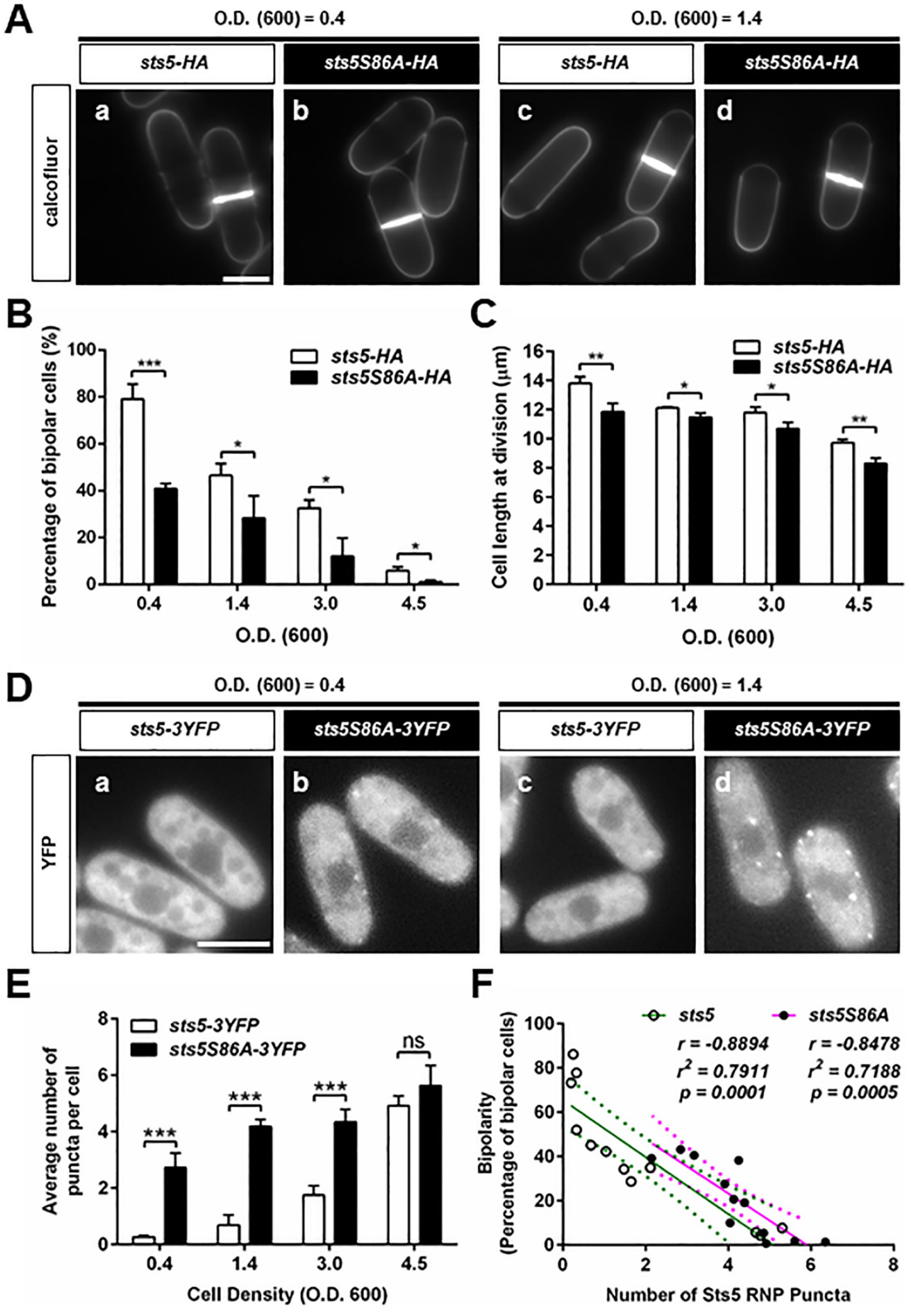

FIGURE 5: The "constitutively coalesced" Sts5S86A mutant protein enhances morphological adaptation during entry into quiescence. (A) *sts5S86A-HA* cells (b and d) display an early change in morphology and growth pattern in response to nutritional stress induced by high cell density from *sts5-HA* control cells (a and c). Cells were stained with calcofluor. Scale bar = 5 μm. (B) Quantification of the percentage of bipolar cells in *sts5-HA* controls vs. *sts5S86A-HA* cells in the experiments depicted in A based on three independent experiments. Percentage of bipolar cells was significantly lower in *sts5S86A-HA* cells than in *sts5-HA* control cells under exponential growth ($OD_{600} < 0.4$) and nutritional stress conditions induced by high cell density ($OD_{600} = 1.4, 3.0, 4.5$). Cells undergoing cell division were not included. Data are presented as mean ± SD; p values are determined by two-tailed Student's *t* test at each condition. $*p < 0.05$,

relative distribution of Scd1 and Gef1 at the cell membrane may control Cdc42 oscillatory dynamics (Das *et al*., 2012), exploratory behavior during mating (Bendezu and Martin, 2013; Khalili *et al*., 2018), and stress response (Mutavchiev *et al*., 2016; Vjestica *et al*., 2013).

Additionally, Orb6 kinase stimulates polarized cell growth through phosphorylation of mRNA binding protein Sts5 by promoting the translation of specific mRNAs (Nuñez *et al*., 2016) whose untranslated regions (UTRs) contain a conserved consensus sequence (Hogan *et al*., 2008; Wanless *et al*., 2014). These mRNAs encode proteins with crucial roles in polarized cell growth, such as conserved signaling kinases (Koyano *et al*., 2010) and exocyst complex subunits such as Sec5 (Nuñez *et al*., 2016). Most recently, Orb6 kinase has been proposed to control cell polarity in a Gef1-independent manner, by phosphorylating Sec3 and Sec5 and thereby promoting exocytosis (Tay *et al*., 2019); however, Orb6 inhibition phenotypes are not suppressed by phosphomimetic mutant alleles (*sec3-S201D/E* or *sec5-S50D/E*) of exocyst complex subunits (Tay *et al*., 2019). In contrast, loss of sts5 (*sts5*Δ) suppresses most aspects of Orb6 inhibition phenotypes, including defects in cell separation, polarized cell growth, and loss of cell viability (Nuñez *et al*., 2016). This suggests that Sts5 is the major regulatory hub, functioning downstream of Orb6 kinase. It is also plausible that exocytosis is promoted by Orb6 at multiple levels, through both translational control and direct phosphorylation of exocyst complex subunits. Via all these mechanisms, increasing or decreasing Orb6 kinase activity promotes, respectively, more or less polarized cell growth (see the model in Figure 7).

Striking a balance between the opposing demands of promoting cell growth and extending chronological lifespan

Nutrient starvation, such as nitrogen depletion, induces fission yeast cells to enter a quiescent state (Su *et al*., 1996). The type of metabolism that occurs before fission yeast cells reach a stationary phase affects cell resilience and viability during cell quiescence (Zuin *et al*., 2010). Sty1 MAP kinase, functioning downstream of the PKA pathway, plays a pivotal role in promoting cell survival following nitrogen depletion (Zuin *et al*., 2010). Deletion of *tor1*, encoding the TOR kinase in the *S. pombe* TORC2 complex, also extends lifespan (Ohtsuka *et al*., 2013). PP2A phosphatase also plays an important role in the nutritional control of cell size, the onset of quiescence, and cell viability during nutritional stress (Chica *et al*., 2016; Martin and Lopez-Aviles, 2018; Aono *et al*., 2019). PP2A activity is down-regulated during nitrogen starvation by the conserved greatwall–endosulfine (Ppk18–Igo1 in fission yeast) pathway (Chica *et al*., 2016) and by the PP2A-type phosphatase inhibitor Sds23 (Hanyu *et al*., 2009).

Here, we report a novel regulator of lifespan, NDR kinase Orb6. Down-regulation of Orb6 promotes cell robustness during quiescence and extension of lifespan, in part, via Sts5-mediated RNP assembly. Adaptation to nutritional stresses relies on mechanisms changing the physical properties of cytoplasm (solidification and fluidization) and modulating key metabolic pathways (Rabouille and Alberti, 2017). Future research will aim to characterize the role of upstream stress-sensing pathways in the control of NDR/LATS kinase activity and the effect of NDR/LATS kinase on phase transition in the cytoplasm. Identifying genetic functions that modulate the phenotype of *sts5* mutants, *sts5Δ* or *stsS86A*, will be particularly useful in defining the novel mechanisms that promote survival during stress.

Our results suggest that modulating the activity of Orb6 kinase in response to nutrient availability allows cells to strike a balance between promoting polarized cell growth in rich media and enhancing cell survival during stress (see the model in Figure 7). We show that increasing Orb6 kinase activity (by expression of Orb6T456D) augments Ras1 activity, fostering bipolar growth and promoting faster recovery in rich media. These phenotypes come with a price, however: during starvation, *orb6T456D* cells are less adaptive and display decreased lifespan. Conversely, decreasing Orb6 kinase phosphorylation of Sts5 suppresses Ras1 activity, leading to monopolar growth and decreasing the rate of recovery in rich media. However, *orb6-as2* cells enjoy an extended lifespan and increased resilience during starvation. Consistent with these results, *sts5Δ* or *sts5S86A* mutants mimic the effects of increased or decreased Orb6 activity, respectively, on lifespan and cell growth (Figure 7).

Overall, these observations suggest that Orb6 kinase is a key controller of cell adaptation, since we can modulate Orb6 kinase activity to either accelerate or decelerate polarized cell growth, and to either extend or reduce chronological lifespan. Importantly, our data also show that wild-type cells display intermediate rates of lifespan extension during stress or cell growth during recovery, suggesting that wild-type cells tend to follow the "Goldilocks principle," existing under "just right" conditions, leaving themselves the opportunity to adapt by either promoting growth or increasing resilience based on changing nutritional conditions.

***$p < 0.001$. (C) Quantification of cell size (defined as cell length at division) in *sts5-HA* control vs. *sts5S86A-HA* cells in the experiments depicted in A based on three independent experiments. Cell size was significantly decreased in *sts5S86A-HA* cells from that of sts5-HA control cells under exponential growth ($OD_{600} < 0.4$) and nutritional stress conditions induced by high cell density ($OD_{600} = 1.4, 3.0, 4.5$). Data are presented as mean ± SD; *p* values are determined by two-tailed Student's *t* test under each condition. *$p < 0.05$, **$p < 0.01$. (D) *sts5S86A-3YFP* cells (b and d) display increased cytoplasmic puncta formation during exponential cell proliferation and during nutritional stress induced by high cell density compared with *sts5-3YFP* control (a and c). Images are deconvolved projections from six Z-stacks separated by a step size of 0.3 µm. Scale bar = 5 µm. (E) Quantification of cytoplasmic puncta numbers per cell in *sts5-3YFP* controls vs. *sts5S86A-3YFP* cells in the experiments depicted in D based on three independent experiments. The average number of puncta per cell was significantly increased in *sts5S86A-3YFP* cells as compared with *sts5-3YFP* control under exponential growth ($OD_{600} < 0.4$) and nutritional stress conditions induced by high cell density ($OD_{600} = 1.4, 3.0, 4.5$). Data are presented as mean ± SD; *p* values are determined by two-tailed Student's *t* test under each condition. ***$p < 0.001$. ns, not statistically significant. (F) Cell bipolarity and number of Sts5 RNP puncta exhibit a strong negative correlation in both control *sts5* cells (black circles, $r = -0.8894$, $p = 0.0001$) and mutant *sts5S86A* cells (black dots, $r = -0.8478$, $p = 0.0005$). Each dot represents one independent experiment with a population of at least 20 cells. The best line fitted with linear regression in *sts5* cells (green solid line) and that in *sts5S86A* cells (magenta solid line) show no statistical significance ($p_{slope} = 0.8538$, $p_{intercept} = 0.1311$). The dashed lines denote 95% confidence interval. Three independent experiments were performed. Correlations were evaluated using the Pearson *r* method.

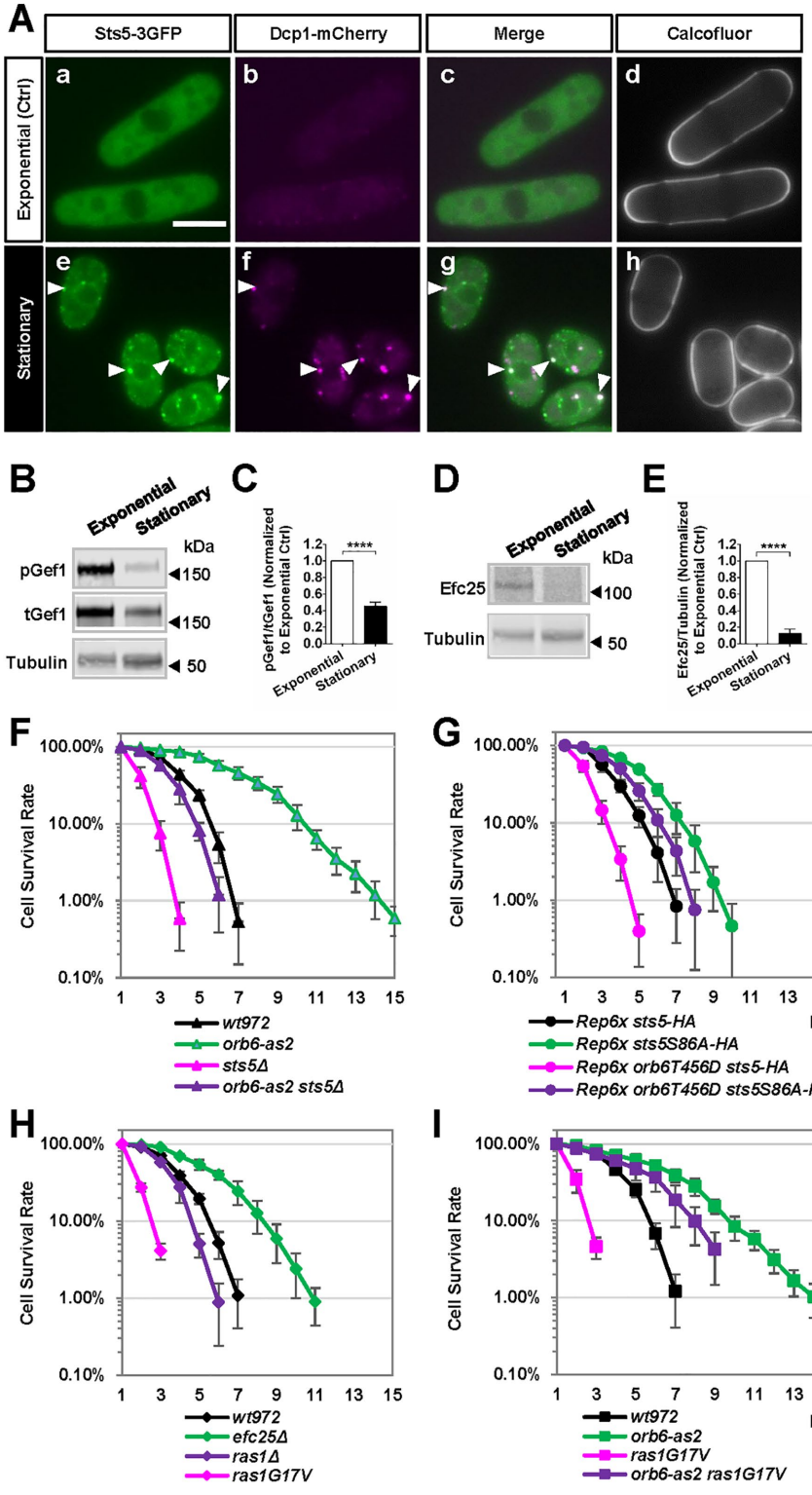

FIGURE 6: Down-regulation of the Orb6–Sts5–Ras1 axis promotes cell survival and extends chronological lifespan during cell quiescence. (A) Sts5-3GFP RNP granules assemble in the stationary phase. *sts5-3GFP dcp1-mCherry* cells are cultured in YE medium at 30°C. In the exponential phase, Sts5-3GFP and Dcp1-mCherry are diffusely located in the cytoplasm (a–c) and the cells exhibit cylindrical shape (d). In the stationary phase, Sts5-3GFP forms cytoplasmic RNP puncta that colocalize with the P-bodies, as visualized by the P-body marker Dcp1-mCherry (e–g), and the cells are decreased in length (h). Scale bar = 5 μm. (B) Orb6 kinase activity decreases in the stationary phase. Western blotting using antibodies to visualize phosphorylated Gef1S112 (pGef1) and YFP-tagged total Gef1 (tGef1) was performed in gef1-3YFP cells cultured in YE medium at 30°C during the exponential cell proliferation phase or the stationary phase. Tubulin levels were determined as a loading control. (C) Quantification of pGef1/tGef1 ratio normalized to exponential phase depicted in B based on three independent experiments. The level of phosphorylated Gef1S112 is significantly decreased in the stationary phase from the exponential phase. Data are presented as mean ± SD; *p* values are determined by two-tailed Student's *t* test. ****$p < 0.0001$. (D) Myc-Efc25 protein level decreases in stationary phase. Western blotting using an anti-Myc antibody to visualize Myc-Efc25 was performed in *myc-efc25* cells cultured in YE medium at 30°C during the exponential cell proliferation phase or the stationary phase. Tubulin levels were determined as a loading control. (E) Quantification of Myc-Efc25/tubulin normalized to the exponential phase depicted in D was based on three independent experiments. The level of Myc-Efc25 is significantly decreased in the stationary phase from the exponential cell proliferation phase. Data are presented as mean ± SD; *p* values are determined by two-tailed Student's *t* test. ****$p < 0.0001$. (F) Decreased Orb6 protein level promotes chronological lifespan in an *sts5*-dependent manner. Colony forming–unit assay was performed in *wt972* control, *orb6-as2*, *sts5*Δ, and *orb6-as2 sts5*Δ cells grown in YE media at 30°C. Down-regulation of Orb6 (*orb6-as2*) promotes cell viability following nutritional stress as compared with the *wt972* control. This increase in lifespan is dependent on *sts5*, as shown by the decreased cell viability in the double-mutant *orb6-as2 sts5*Δ cells. *sts5*Δ single-mutant cells exhibit decreased viability under nutritional stress. Quantification of cell survival rate was based on three independent experiments. Data are presented as mean ± SD. (G) Colony forming–unit assay was performed in *Rep6x sts5-HA* controls, *Rep6 sts5S86A-HA*, *Rep6xorb6T456D sts5-HA*, and *Rep6xorb6T456D sts5S86A-HA* cells grown in YE medium at 30°C. Compared with the *Rep6x sts5-HA* control cells, the constitutively active Orb6 mutant *Rep6xorb6T456D sts5-HA* exhibit decreased cell viability under nutritional stress. *sts5S86A* mutation exhibits prolonged lifespan compared with the control and suppresses the decrease in lifespan of *Rep6xorb6T456D* cells. Quantification of cell survival rate was based on three independent experiments. Data are presented as mean ± SD. (H) Decreased Ras1 activity promotes lifespan. Colony forming–unit assay was performed in *wt972* control and *efc25*Δ cells grown in YE medium at 30°C. Compared with the *wt972* controls, the *efc25*Δ cells exhibit increased viability under nutritional stress, while the constitutively active Ras1 mutant *ras1G17V* shows decreased viability. *ras1*Δ cells do not exhibit increased viability. Quantification of cell survival rate was based on three independent experiments. Data are presented as mean ± SD. (I) Colony forming–unit assay was performed in *wt972* controls, *orb6-as2*, *ras1G17V*, and *orb6-as2 ras1G17V* cells grown in YE medium at 30°C. Compared with the *orb6-as2* cells, the *orb6-as2 ras1G17V* double-mutant cells exhibit decreased cell viability under nutritional stress. Quantification of cell survival rate was based on three independent experiments. Data are presented as mean ± SD.

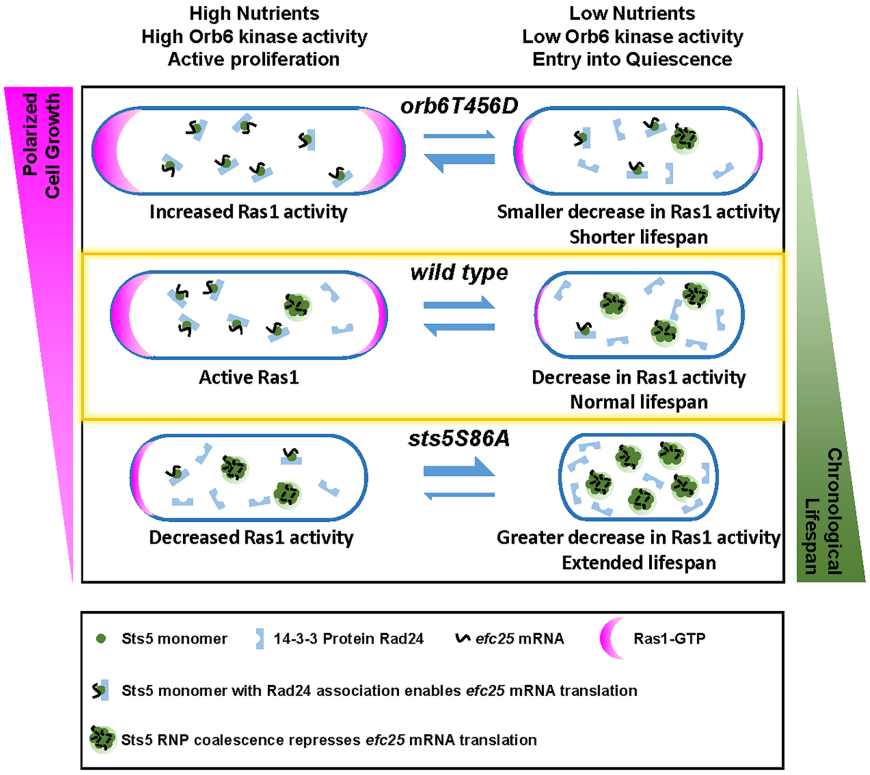

FIGURE 7: Model of Orb6 kinase balancing the opposing demands of promoting polarized cell growth and extending chronological lifespan. During nutritional abundance, Orb6 kinase (wild type) is active. Orb6 phosphorylates Sts5 at Ser-86 and promotes Sts5 association with the 14-3-3 protein Rad24, thereby inhibiting Sts5 assembly into RNP granules. By this mechanism, Ras1 GEF Efc25 protein level increases and Ras1 activity is promoted. Constitutively active Orb6 kinase (*orb6T456D*) decreases Sts5 RNP assembly, thereby increasing Ras1 activity at the cell tips and promoting bipolar cell growth. Conversely, the constitutively coalesced mutant (*sts5S86A*), expressing a nonphosphorylated Sts5S86A protein, displays increased Sts5 RNP assembly, decreased Ras1 activity at the cell tips, and decreased bipolar cell growth. During nutritional deprivation, Orb6 kinase activity decreases. Dephosphorylation of Sts5 at Ser-86 dissociates 14-3-3 protein Rad24 binding with Sts5, thereby promoting Sts5 RNP granule assembly. By this mechanism, Ras1 GEF Efc25 protein decreases and Ras1 GTPase activity is down-regulated. Decreased Ras1 activity at cell tips fosters entry into quiescence (blue arrows toward the right) and increases lifespan. Consistent with a decreased extent of Sts5 RNP assembly, the constitutively active *orb6T456D* mutant displays a shorter lifespan, while the constitutively coalesced *sts5S86A* mutant displays a longer lifespan during quiescence. During recovery from nutritional deprivation (blue arrows toward the left), the constitutively active *orb6T456D* mutant displays faster recovery. Conversely, recovery is delayed in the constitutively coalesced *sts5S86A* mutant cells, consistent with the rate of recovery being dependent, at least in part, on the dissolution of Sts5 RNP granules. By the Orb6-Sts5-Ras1 regulatory mechanism, the opposing demands of promoting cell growth and increasing chronological lifespan are balanced in response to nutrient fluctuations. As highlighted by the yellow rectangle, wild-type cells exist in an intermediate state between the extremes observed in constitutively active *orb6T456D* and constitutively coalesced *sts5S86A* mutants, as far as the extent of Sts5 granule assembly, Ras1 activity, and chronological lifespan are concerned. This suggests that wild-type cells live under "just right" conditions, leaving themselves the opportunity to adapt by either promoting cell growth or increasing cell adaptiveness based on changing nutritional conditions.

Genes and signaling pathways regulating chronological lifespan in yeast share remarkable similarities to those in higher organisms, including worms, flies, and mammals (Longo *et al.*, 2012; Lin and Austriaco, 2014). Interestingly, pharmacological inhibition of RAS signaling in *Drosophila* is sufficient for organism lifespan extension, which may provide targets for anti-aging interventions in mammals (Slack *et al.*, 2015). Consistently, mice with loss of *RasGrf1*, encoding the Ras guanine nucleotide exchange factor RASGRF1, display increased lifespan with better motor coordination and metabolic profiles (Borras *et al.*, 2011). By showing that the NDR kinase Orb6 regulates RAS activity through a fundamental mechanism such as RNP-mediated translational repression, our studies may unveil a novel lifespan regulation pathway in higher eukaryotes.

The other biological process regulated by NDR kinase Orb6 is cell growth, in a manner that is partially dependent on the mRNA binding protein Sts5. Intriguingly, germline mutations in human *Dis3L2*, encoding the closest human homologue of *S. pombe* Sts5, cause the Perlman syndrome of overgrowth and Wilms tumor susceptibility (Astuti *et al.*, 2012) by increasing the abundance of mRNAs with roles in the cell cycle (Lubas *et al.*, 2013), cell homeostasis (Labno *et al.*, 2016), and cell growth (Hunter *et al.*, 2018). Moreover, mammalian YAP/TAZ transcriptional coactivators, established targets of NDR/LATS kinases in the Hippo cascade (Zhang *et al.*, 2015; Hergovich, 2016), regulate cell metabolism and cell proliferation in response to nutrient availability (Koo and Guan, 2018).

Thus, our findings unveil a novel, significant role of the Orb6–Sts5–Ras1 regulatory axis in regulating cell adaptation during active cell proliferation and during cell quiescence, highlighting the conserved NDR/LATS kinase as a crucial enzyme in modulating cell growth and chronological lifespan under favorable or nutritionally stressful conditions.

MATERIALS AND METHODS

Strains and cell culture

S. pombe strains used in this study are listed in Table 1. All strains used in this study are isogenic to the original strain 972. Fission yeast cells were cultured in YE medium or Edinburgh minimal medium (EMM) plus required supplements unless otherwise specified. Cells used in nitrogen starvation experiments were prototrophic and were cultured in unsupplemented EMM plus or minus 0.5% nitrogen resource (NH_4Cl). Cells used in colony forming–unit assay were prototrophic and were cultured in YE medium. Exponential growth was maintained for at least eight generations before experiments, and genetic manipulations and analyses were carried out following standard techniques (Moreno *et al.*, 1991). We used monoclonal anti-alpha-tubulin antibody produced in the mouse (Sigma-Aldrich Cat# T5168) to visualize the protein loading. We used anti-GFP antibody (Sigma-Aldrich Cat# 11814460001) to visualize GFP- or YFP-tagged proteins.

Development of anti-pGef1S112 phosphospecific antibody

The anti-pGef1S112 phosphospecific antibody was custom-made by 21st Century Biochemicals against a synthetic peptide corresponding to the phosphorylated Ser-112 (amino acids 102–122,

Strains	Genotype	Origin
PN972	*h-*	Leupold, 1949
FV1108	*h- ade6-706 leu1-32 ura4-D18*	This paper
FV2707	*h-* RasAct-3GFP::leu+ leu1-32 ade- ura-	Merlini *et al.*, 2018
FV2719	*orb6Δ::ura+ pJK148orb6-as2::leu+ RasAct-3GFP::leu+ ade-*	This paper
FV2923	*orb6Δ::ura+ pJK148orb6-as2::leu+ RasAct-3GFP::leu+ sts5Δ::KanMX6 ade-*	This paper
FV2740	*scd1-3GFP:KanMX6*	This paper
FV2744	*h- scd1-3GFP:KanMX6 orb6Δ::ura+ pJK148orb6-as2::leu+*	This paper
FV2763	*sts5Nterm-3YFP::KanMX6 dcp1-mCherry::hph*	This paper
FV0558	*h- mob2-13Myc:kanMX6 ura4-D18 leu1-32 ade6-*	Nuñez *et al.*, 2016
FV2645	*h- sts5Δ::NatMX6 sts5-HA::KanMX6*	This paper
FV2649	*h+ sts5Δ::NatMX6 sts5S86A-HA::KanMX6*	This paper
FV2685	*sts5Δ::NatMX6 sts5-HA::KanMX6 c-myc-efc25 efc25Δ::ura+ ars1::EPcM-efc25-LEU2 ade210 leu1-32 ura4-D18*	This paper
FV2687	*sts5Δ::NatMX6 sts5S86A-HA::KanMX6 c-myc-efc25 efc25Δ::ura+ ars1::EPcM-efc25-LEU2 ade210 leu1-32 ura4-D18*	This paper
FV1507	*orb4-A9 c-my- efc25 efc25Δ::ura4+ ars1::EPcM-efc25-LEU2 ade210 leu1-32 ura4-D18*	Nuñez *et al.*, 2016
FV2750	*RasAct-3GFP::leu+ sts5Δ::NatMX6 sts5-HA::KanMX6 leu1-32*	This paper
FV2754	*RasAct-3GFP::leu+ sts5Δ::NatMX6 sts5S86A-HA::KanMX6 leu1-32*	This paper
FV2758	*RasAct-3GFP::leu+ sts5Δ::NatMX6*	This paper
FV2518	*sts5Δ::NatMX6 sts5-HA::KanMX6*	This paper
FV2522	*sts5Δ::NatMX6 sts586A-HA::KanMX6*	This paper
FV2713	*h- RasAct-3GFP::leu+ leu1-32*	This paper
FV2206	*gef1Δ::NatMX6 gef1-3YFP::KanMX6*	This paper
FV2875	*efc25Δ::ura+ c-myc-efc25 ars1::EPcM-efc25-LEU2*	This paper
FV2917	*sts5Δ::KanMX6 efc25Δ::ura+ c-myc-efc25 ars1::EPcM-efc25-LEU2*	This paper
FV2877	*pRep6X sts5Δ::NatMX6 sts5-HA::KanMX6 RasAct-3GFP::leu+ leu1-32*	This paper
FV2865	*pRep6Xorb6T456D sts5Δ::NatMX6 sts5-HA::KanMX6 RasAct-3GFP::leu+*	This paper
FV2817	*pRep6Xorb6T456D sts5Δ::NatMX6 sts5S86A-HA::KanMX6 RasAct-3GFP::leu+*	This paper
FV2267	*sts5-3GFP::NatMX6 dcp1-mCherry::hph*	This paper
FV2527	*h- orb6Δ::ura4+ pJK148orb6-as2:leu1+*	This paper
FV2674	*sts5Δ::KanMX6*	This paper
FV2672	*orb6Δ::ura4+ pJK148orb6-as2:leu1+ sts5Δ::KanMX6*	This paper
FV2895	*efc25Δ::KanMX6*	This paper
FV2911	*ras1Δ::KanMX6*	This paper
FV2828	*ras1G17V::ura+ ura4-D18*	This paper
FV2957	*pRep6X sts5-HA::KanMX sts5Δ::NatMX6 ade-*	This paper
FV2965	*pRep6X sts5S86A-HA::KanMX sts5Δ::NatMX6 ade-*	This paper
FV2961	*pRep6Xorb6T456D sts5-HA::KanMX sts5Δ::NatMX6 ade-*	This paper
FV2821	*pRep6Xorb6T456D sts5S86A-HA::KanMX sts5Δ::NatMX6 ade-*	This paper
FV2923	*sts5Δ::KanMX6 orb6Δ::ura+ pJK148orb6-as2::leu+ RasAct-3GFP::leu+ ade-*	This paper
FV2938	*ras1Δ::ura+ scd1-3GFP::KanMX6 ade210 leu1-32 ura4-D18*	This paper
FV2805	*pRep6X gef1Δ::NatMX6 gef1-3YFP::KanMX6 ade-*	This paper
FV2809	*pRep6Xorb6 gef1Δ::NatMX6 gef1-3YFP::KanMX6 ade-*	This paper
FV2813	*pRep6Xorb6T456D gef1Δ::NatMX6 gef1-3YFP::KanMX6 ade-*	This paper
FV2972	*pRep6X sts5-3YFP::KanMX6 ade-*	This paper
FV2974	*pRep6Xorb6T456D sts5-3YFP::KanMX6 ade-*	This paper

TABLE 1: Strains.

PVSSQHRRFFS*EGSFNLPNSN) of the fission yeast Gef1 protein. To achieve antibody specificity for the phosphorylated form of Gef1S112, a nonphosphopeptide with the same sequence was manufactured and used for immunodepletion of the serum of antibodies that are phosphorylation state–independent. These antibodies underwent a nonphosphopeptide depletion column and were removed before affinity purification of the phosphospecific antibody.

We observed that a residual weak signal remains in the presence of 1-NA-PP1, and that on the average, inhibitor addition decreases the Gef1p signal by 60% in the *nmt1* promoter–driven *orb6-as2* mutant cells. This effect could be due to incomplete kinase inhibition by the inhibitor. While complete loss of the *orb6* gene leads to cell death, we do observe very slow cell growth in the presence of inhibitor (unpublished data).

Fluorescence microscopy

Cells expressing fluorescently tagged proteins were photographed with an Olympus fluorescence BX61 microscope (Melville, NY) equipped with Nomarski differential interference contrast (DIC) optics, a 100× objective (numerical aperture [NA] 1.35), a Roper CoolSNAP HQ camera (Tucson, AZ), Sutter Lambda 10 + 2 automated excitation and emission filter wheels (Novato, CA), and a 175-W Xenon remote source lamp with liquid light guide. Images were acquired and processed using Intelligent Imaging Innovations SlideBook image analysis software (Version 6.0.11; Denver, CO) and prepared with Fiji (Schindelin *et al.*, 2012). For the measurements of Sts5-3GFP puncta intensity or tip RasAct-3GFP and Scd1-3GFP intensity, we subtracted the cytoplasmic background for each cell as previously described (Das *et al.*, 2012; Nuñez *et al.*, 2016). The subtraction was performed by using an ImageJ plug-in that sets a subtraction threshold to three standard deviations from the cytoplasmic-region mean. The number of Sts5 puncta after background subtraction was scored manually (Nuñez *et al.*, 2016). The scoring method due to the application of the threshold may ignore smaller puncta.

Construction of Sts5 mutant strains

Cloning and transformation were performed as previously described (Nuñez *et al.*, 2016). Briefly, Sts5 promoter was cloned along with either the full-length Sts5 gene or the N-terminus of the Sts5 gene (from position 1 to position 852) into the pFA6-HA and pFA6-3YFP plasmid and placed in the *sts5*Δ mutant. The *sts5S86A* mutant was generated by site-directed mutagenesis using a QuickChange Kit (Stratagene, La Jolla, CA). The construct was then transformed into FV2321 (*sts5::NatMX leu1-32 ura4-D18 ade6-704*) cells, selecting for G418-resistant colonies. The resulting strain contained one functional copy of *sts5* full length or N-terminus with or without S86A mutation fused to HA or 3YFP followed by *sts5::NatMX* sequence.

Bacterial expression and purification of mutant Sts5 protein

Bacterial expression and purification were performed following previously established methods (Nuñez *et al.*, 2016). Briefly, full-length Sts5 (amino acids 1–1066) or truncated (amino acids 1–284) Sts5 N-terminus with or without S86A mutation was tagged with N-terminal His6 by cloning into a pET-15b expression vector. The construct was transformed into Rosetta cells, and His6-Sts5Nterm expression was induced by incubation with 1 mM IPTG for 1 h. Native His6-Sts5 was purified using Ni-NTA spin columns (Qiagen) following the manufacturer's instructions. Western blot using anti-His6 antibody (Covance; AB_10063707) was performed to confirm the purification of His6-Sts5.

Mob2-associated kinase assay

Purification of Mob2-associated Orb6 kinase was performed using previously established methods (Wiley *et al.*, 2003; Nuñez *et al.*, 2016) and in vitro thiophosphorylation assay was optimized from published protocols (Allen *et al.*, 2007; Hertz *et al.*, 2010; Opalko and Moseley, 2017; Lee *et al.*, 2018). Briefly, Myc-tagged Mob2 and untagged Mob2 were expressed in *S. pombe* cells grown to mid-log phase at 30°C. Cells were lysed using Savant FastPrep FP120 bead beater in HB buffer (25 mM MOPS, pH 7.2, 60 mM β-glycerophosphate, 15 mM p-nitrophenyl phosphate, 15 mM $MgCl_2$, 15 mM EGTA [ethylene glycol-bis(β-aminoethyl ether)-*N*,*N*,*N*′,*N*′-tetraacetic acid], 1 mM dithiothreitol, 0.1 M sodium vanadate, 1% Triton X-100, 1 mM phenylmethylsulfonyl fluoride [PMSF], and complete EDTA-free protease inhibitor cocktail tablets [Roche Applied Science]). Extracts from cells expressing Myc-tagged Mob2 and from wild-type cells were incubated with Protein A agarose beads (Sigma-Aldrich) bound to rabbit anti-Myc antibodies (Santa Cruz Biochenology; RRID: AB_631274) for 1 h, washed twice with HB buffer, and then washed once with kinase buffer (50 mM Tris-HCl, pH 7.5, 100 mM NaCl, 10 mM $MgCl_2$, 1 mM $MnCl_2$). The resin was resuspended in 25 µl of kinase buffer containing 1 mM ATPγS and combined with 5 µl bacterially expressed Sts5Nterm. The kinase reaction was stopped after 30 min at 30°C by adding 20 mM EDTA and alkylated by incubating with 2.5 mM *p*-nitrobenzylmesylate (abcam #ab138910) for 1.5 h. Proteins were separated on an SDS polyacrylamide gel and the thiophosphate ester was detected by a rabbit monoclonal antibody (abcam #ab92570).

Rad24 binding assay

The Rad24 binding assay was performed as previously described (Das *et al.*, 2015; Nuñez *et al.*, 2016). Briefly, bacterially expressed GST and GST-Rad24 were bound to glutathione-linked magnetic beads (Piece, Rockford, IL). Then the beads were mixed with fission yeast protein extract from *sts5-HA* and *sts5S86A-HA* strains and incubated overnight at 4°C. The beads were washed with Tris lysis buffer (50 mM Tris-Cl, pH 7.7, 150 mM NaCl, 5 mM EDTA, 5% glycerol, 1% Triton X, 1 mM PMSF, complete EDTA-free protease inhibitor cocktail tablets [Roche Applied Science]) and the protein was separated by SDS polyacrylamide gel and analyzed by Western blot, using mouse monoclonal anti-HA antibodies (Covance; RRID: AB_2314672).

Orb6-as2 kinase inhibition

Design and construction of the *orb6-as2* analogue-sensitive mutant were as previously described (Das *et al.*, 2009). Inhibition of Orb6-as2 kinase was achieved using the ATP analogue 1-NA-PP1 (4-amino-1-tert-butyl-3-(1′-naphtyl) pyrazolo [3,4-d]pyrimidine; Toronto Research Chemicals) diluted in DMSO. In liquid media, the final concentration of 1-NA-PP1 used was 50 µM.

Nitrogen starvation

All strains used in nitrogen starvation experiments were prototrophic and were cultured in unsupplemented EMM to eliminate the effect of supplemented amino acids as potential nitrogen resources. Therefore, the starvation and refeeding of the nitrogen resource in this study was achieved by removal and addition of 0.5% NH_4Cl, respectively. For starvation experiments, cells cultured in EMM+0.5% NH_4Cl (EMM+N) were spun down, washed once in EMM+0% NH_4Cl (EMM-N), and resuspended in either EMM+0.5% NH_4Cl (EMM+N) as a control or EMM+0% NH_4Cl (EMM-N) for study. For nitrogen refeeding experiments, cells were first starved of nitrogen as described above for 16 h. Then cells were spun down and resuspended in EMM+N.

Colony forming–unit (CFU) assay

The colony forming–unit assay was performed as previously described with modifications (Fabrizio *et al.*, 2001; Roux *et al.*, 2006, 2009; Wei *et al.*, 2008; Rallis *et al.*, 2013). Briefly, cells cultured in YE medium were harvested, diluted, and plated on YE agar plates 24 and 48 h after the optical density reached maximum; the larger number of colonies coming up on plates from these two samples was considered as Day 1 (the beginning of the chronological lifespan curve with survival rate 100%). Measurements of CFUs were conducted each day on the following days until living colonies of the culture declined to around 0.1% of the initial cell survival or no colonies survived, whichever came first. Error bars represent SD calculated from three independent cultures. Construction of *orb6-as2* mutant was previously described (Das *et al.*, 2009). This allele is integrated in the genome in single copy under the thiamine-responsive *nmt1* promoter; its expression level in YE media that contains thiamine is decreased (Das *et al.*, 2009).

Heatmap of RasAct-3GFP tip fraction

The R code for plotting the tip fraction of RasAct-3GFP is as follows:

```
library("readxl");
file ← read_excel("20190107 HM Ratio.xlsx");
data ← file[,c(2:4)];
rownames(data) ← file$genotype;
pheatmap(data, cluster_row = FALSE,color = colorRampPalette(c("white","black"))(50))
```

Quantification and statistical analysis

Data are expressed as mean ± SD. Exact numbers (n) of independent experiments repeated are noted in each figure legend. A two-tailed unpaired Student's t test was used to assess statistical significance between two groups. One-way analysis of variance (ANOVA) followed by a Dunnett (comparison relative to control) or Tukey (multiple comparisons between groups) post hoc test was applied to evaluate the difference between three or more groups. Correlations were assessed using the Pearson r method. Statistical analyses and visualization were performed with IBM SPSS Statistics, Version 24.0. (IBM, Armonk, NY), GraphPad Prism 6 (GraphPad Software, San Diego, CA), and R (R, Boston, MA). p value < 0.05 was set as the threshold for statistical significance.

ACKNOWLEDGMENTS

We thank Sophie G. Martin (University of Lausanne, Lausanne, Switzerland) and Arun Malhotra (University of Miami, Miami, FL) for providing strains and plasmids. We thank Sandra Lemmon (University of Miami, Miami, FL) and Maitreyi Das (University of Tennessee, Knoxville, TN) for critical review of the manuscript. We thank April Mann (University of Miami, Miami, FL) for comments on the manuscript. We thank Qin Yang (University of Miami, Miami, FL) for technical support in data visualization. This work in F.V.'s laboratory was supported by National Institutes of Health R01 Grant GM095867 and by the Sylvester Comprehensive Cancer Center.

REFERENCES

Adeyinka A, Emberley E, Niu Y, Snell L, Murphy LC, Sowter H, Wykoff CC, Harris AL, Watson PH (2002). Analysis of gene expression in ductal carcinoma in situ of the breast. Clin Cancer Res 8, 3788–3795.

Allen JJ, Li M, Brinkworth CS, Paulson JL, Wang D, Hubner A, Chou WH, Davis RJ, Burlingame AL, Messing RO, *et al.* (2007). A semisynthetic epitope for kinase substrates. Nat Methods 4, 511–516.

Ambadipudi S, Biernat J, Riedel D, Mandelkow E, Zweckstetter M (2017). Liquid-liquid phase separation of the microtubule-binding repeats of the Alzheimer-related protein Tau. Nat Commun 8, 275.

Aono S, Haruna Y, Watanabe YH, Mochida S, Takeda K (2019). The fission yeast Greatwall–Endosulfine pathway is required for proper quiescence/G0 phase entry and maintenance. Genes Cells 24, 172–186.

Astuti D, Morris MR, Cooper WN, Staals RH, Wake NC, Fews GA, Gill H, Gentle D, Shuib S, Ricketts CJ, *et al.* (2012). Germline mutations in DIS3L2 cause the Perlman syndrome of overgrowth and Wilms tumor susceptibility. Nat Genet 44, 277–284.

Aumiller WM Jr, Keating CD (2016). Phosphorylation-mediated RNA/peptide complex coacervation as a model for intracellular liquid organelles. Nat Chem 8, 129–137.

Becker LA, Gitler AD (2015). It's all starting to come together. eLife 4, doi: 10.7554/eLife.09853.

Bendezu FO, Martin SG (2013). Cdc42 explores the cell periphery for mate selection in fission yeast. Curr Biol 23, 42–47.

Borras C, Monleon D, Lopez-Grueso R, Gambini J, Orlando L, Pallardo FV, Santos E, Vina J, Font de Mora J (2011). RasGrf1 deficiency delays aging in mice. Aging 3, 262–276.

Brangwynne CP (2013). Phase transitions and size scaling of membrane-less organelles. J Cell Biol 203, 875–881.

Brangwynne CP, Eckmann CR, Courson DS, Rybarska A, Hoege C, Gharakhani J, Julicher F, Hyman AA (2009). Germline P granules are liquid droplets that localize by controlled dissolution/condensation. Science 324, 1729–1732.

Chang EC, Barr M, Wang Y, Jung V, Xu HP, Wigler MH (1994). Cooperative interaction of *S. pombe* proteins required for mating and morphogenesis. Cell 79, 131–141.

Chica N, Rozalen AE, Perez-Hidalgo L, Rubio A, Novak B, Moreno S (2016). Nutritional control of cell size by the Greatwall–Endosulfine–PP2A.B55 pathway. Curr Biol 26, 319–330.

Chiou JG, Balasubramanian MK, Lew DJ (2017). Cell polarity in yeast. Annu Rev Cell Dev Biol 33, 77–101.

Coll PM, Trillo Y, Ametzazurra A, Perez P (2003). Gef1p, a new guanine nucleotide exchange factor for Cdc42p, regulates polarity in *Schizosaccharomyces pombe*. Mol Biol Cell 14, 313–323.

Cornils H, Stegert MR, Hergovich A, Hynx D, Schmitz D, Dirnhofer S, Hemmings BA (2010). Ablation of the kinase NDR1 predisposes mice to the development of T cell lymphoma. Sci Signal 3, ra47.

Costello G, Rodgers L, Beach D (1986). Fission yeast enters the stationary phase G 0 state from either mitotic G 1 or G 2. Curr Genet 11, 119–125.

Das M, Drake T, Wiley DJ, Buchwald P, Vavylonis D, Verde F (2012). Oscillatory dynamics of Cdc42 GTPase in the control of polarized growth. Science 337, 239–243.

Das M, Nuñez I, Rodriguez M, Wiley DJ, Rodriguez J, Sarkeshik A, Yates JR 3rd, Buchwald P, Verde F (2015). Phosphorylation-dependent inhibition of Cdc42 GEF Gef1 by 14-3-3 protein Rad24 spatially regulates Cdc42 GTPase activity and oscillatory dynamics during cell morphogenesis. Mol Biol Cell 26, 3520–3534.

Das M, Wiley DJ, Chen X, Shah K, Verde F (2009). The conserved NDR kinase Orb6 controls polarized cell growth by spatial regulation of the small GTPase Cdc42. Curr Biol 19, 1314–1319.

Decker CJ, Parker R (2012). P-bodies and stress granules: possible roles in the control of translation and mRNA degradation. Cold Spring Harb Perspect Biol 4, a012286.

Elbaum-Garfinkle S, Kim Y, Szczepaniak K, Chen CC, Eckmann CR, Myong S, Brangwynne CP (2015). The disordered P granule protein LAF-1 drives phase separation into droplets with tunable viscosity and dynamics. Proc Natl Acad Sci USA 112, 7189–7194.

Fabrizio P, Longo VD (2003). The chronological life span of *Saccharomyces cerevisiae*. Aging Cell 2, 73–81.

Fabrizio P, Pozza F, Pletcher SD, Gendron CM, Longo VD (2001). Regulation of longevity and stress resistance by Sch9 in yeast. Science 292, 288–290.

Fantes P, Nurse P (1977). Control of cell size at division in fission yeast by a growth-modulated size control over nuclear division. Exp Cell Res 107, 377–386.

Franzmann TM, Alberti S (2019). Protein phase separation as a stress survival strategy. Cold Spring Harb Perspect Biol, doi: 10.1101/cshperspect.a034058.

Hanyu Y, Imai KK, Kawasaki Y, Nakamura T, Nakaseko Y, Nagao K, Kokubu A, Ebe M, Fujisawa A, Hayashi T, *et al.* (2009). *Schizosaccharomyces pombe* cell division cycle under limited glucose requires Ssp1 kinase, the putative CaMKK, and Sds23, a PP2A-related phosphatase inhibitor. Genes Cells 14, 539–554.

Hao Y, Chun A, Cheung K, Rashidi B, Yang X (2008). Tumor suppressor LATS1 is a negative regulator of oncogene YAP. J Biol Chem 283, 5496–5509.
Hauschild A, Engel G, Brenner W, Glaser R, Monig H, Henze E, Christophers E (1999). S100B protein detection in serum is a significant prognostic factor in metastatic melanoma. Oncology 56, 338–344.
Hergovich A (2016). The roles of NDR protein kinases in hippo signalling. Genes 7, doi: 10.3390/genes7050021.
Hergovich A, Stegert MR, Schmitz D, Hemmings BA (2006). NDR kinases regulate essential cell processes from yeast to humans. Nat Rev Mol Cell Biol 7, 253–264.
Hermeking H, Benzinger A (2006). 14-3-3 proteins in cell cycle regulation. Semin Cancer Biol 16, 183–192.
Hertz NT, Wang BT, Allen JJ, Zhang C, Dar AC, Burlingame AL, Shokat KM (2010). Chemical genetic approach for kinase-substrate mapping by covalent capture of thiophosphopeptides and analysis by mass spectrometry. Curr Protoc Chem Biol 2, 15–36.
Hogan DJ, Riordan DP, Gerber AP, Herschlag D, Brown PO (2008). Diverse RNA-binding proteins interact with functionally related sets of RNAs, suggesting an extensive regulatory system. PLoS Biol 6, e255.
Huang X, Leggas M, Dickson RC (2015). Drug synergy drives conserved pathways to increase fission yeast lifespan. PLoS One 10, e0121877.
Hughes DA, Ashworth A, Marshall CJ (1993). Complementation of byr1 in fission yeast by mammalian MAP kinase kinase requires coexpression of Raf kinase. Nature 364, 349–352.
Hughes DA, Yabana N, Yamamoto M (1994). Transcriptional regulation of a Ras nucleotide-exchange factor gene by extracellular signals in fission yeast. J Cell Sci 107(Pt 12), 3635–3642.
Hunter RW, Liu Y, Manjunath H, Acharya A, Jones BT, Zhang H, Chen B, Ramalingam H, Hammer RE, Xie Y, *et al*. (2018). Loss of Dis3l2 partially phenocopies Perlman syndrome in mice and results in up-regulation of Igf2 in nephron progenitor cells. Genes Dev 32, 903–908.
Hyman AA, Weber CA, Julicher F (2014). Liquid–liquid phase separation in biology. Annu Rev Cell Dev Biol 30, 39–58.
Jeyabalan N, Clement JP (2016). SYNGAP1: mind the gap. Front Cell Neurosci 10, 32.
Khalili B, Merlini L, Vincenzetti V, Martin SG, Vavylonis D (2018). Exploration and stabilization of Ras1 mating zone: a mechanism with positive and negative feedbacks. PLoS Comput Biol 14, e1006317.
Koo JH, Guan KL (2018). Interplay between YAP/TAZ and metabolism. Cell Metab 28, 196–206.
Koyano T, Kume K, Konishi M, Toda T, Hirata D (2010). Search for kinases related to transition of growth polarity in fission yeast. Biosci Biotechnol Biochem 74, 1129–1133.
Kroschwald S, Alberti S (2017). Gel or die: phase separation as a survival strategy. Cell 168, 947–948.
Kroschwald S, Maharana S, Mateju D, Malinovska L, Nuske E, Poser I, Richter D, Alberti S (2015). Promiscuous interactions and protein disaggregases determine the material state of stress-inducible RNP granules. eLife 4, e06807.
Kurischko C, Kim HK, Kuravi VK, Pratzka J, Luca FC (2011). The yeast Cbk1 kinase regulates mRNA localization via the mRNA-binding protein Ssd1. J Cell Biol 192, 583–598.
Labno A, Warkocki Z, Kulinski T, Krawczyk PS, Bijata K, Tomecki R, Dziembowski A (2016). Perlman syndrome nuclease DIS3L2 controls cytoplasmic non-coding RNAs and provides surveillance pathway for maturing snRNAs. Nucleic Acids Res 44, 10437–10453.
Larson AG, Elnatan D, Keenen MM, Trnka MJ, Johnston JB, Burlingame AL, Agard DA, Redding S, Narlikar GJ (2017). Liquid droplet formation by HP1alpha suggests a role for phase separation in heterochromatin. Nature 547, 236–240.
Lee CF, Brangwynne CP, Gharakhani J, Hyman AA, Julicher F (2013). Spatial organization of the cell cytoplasm by position-dependent phase separation. Phys Rev Lett 111, 088101.
Lee ME, Rusin SF, Jenkins N, Kettenbach AN, Moseley JB (2018). Mechanisms connecting the conserved protein kinases Ssp1, Kin1, and Pom1 in fission yeast cell polarity and division. Curr Biol 28, 84–92.e84.
Leupold U (1949). Die Vererbung von Homothallie und Heterothallie bei *Schizosaccharomyces pombe*. Compt Rend Trav Lab Carlsberg Ser Physiol 24, 381–480.
Lin SJ, Austriaco N (2014). Aging and cell death in the other yeasts, *Schizosaccharomyces pombe* and *Candida albicans*. FEMS Yeast Res 14, 119–135.
Lin Y, Protter DS, Rosen MK, Parker R (2015). Formation and maturation of phase-separated liquid droplets by RNA-binding proteins. Mol Cell 60, 208–219.
Longo VD, Shadel GS, Kaeberlein M, Kennedy B (2012). Replicative and chronological aging in *Saccharomyces cerevisiae*. Cell Metab 16, 18–31.
Lubas M, Damgaard CK, Tomecki R, Cysewski D, Jensen TH, Dziembowski A (2013). Exonuclease hDIS3L2 specifies an exosome-independent 3′-5′ degradation pathway of human cytoplasmic mRNA. EMBO J 32, 1855–1868.
Lv H, Zhu Y, Qiu Y, Niu L, Teng M, Li X (2015). Structural analysis of Dis3l2, an exosome-independent exonuclease from *Schizosaccharomyces pombe*. Acta Crystallogr D Biol Crystallogr 71, 1284–1294.
Malecki M, Viegas SC, Carneiro T, Golik P, Dressaire C, Ferreira MG, Arraiano CM (2013). The exoribonuclease Dis3L2 defines a novel eukaryotic RNA degradation pathway. EMBO J 32, 1842–1854.
Martin R, Lopez-Aviles S (2018). Express yourself: how PP2A-B55(Pab1) helps TORC1 talk to TORC2. Curr Genet 64, 43–51.
Mazanka E, Alexander J, Yeh BJ, Charoenpong P, Lowery DM, Yaffe M, Weiss EL (2008). The NDR/LATS family kinase Cbk1 directly controls transcriptional asymmetry. PLoS Biol 6, e203.
Merlini L, Khalili B, Dudin O, Michon L, Vincenzetti V, Martin SG (2018). Inhibition of Ras activity coordinates cell fusion with cell-cell contact during yeast mating. J Cell Biol, doi: 10.1083/jcb.201708195.
Mignot C, von Stulpnagel C, Nava C, Ville D, Sanlaville D, Lesca G, Rastetter A, Gachet B, Marie Y, Korenke GC, *et al*. (2016). Genetic and neurodevelopmental spectrum of SYNGAP1-associated intellectual disability and epilepsy. J Med Genet 53, 511–522.
Millward TA, Heizmann CW, Schafer BW, Hemmings BA (1998). Calcium regulation of Ndr protein kinase mediated by S100 calcium-binding proteins. EMBO J 17, 5913–5922.
Mitchison JM, Nurse P (1985). Growth in cell length in the fission yeast *Schizosaccharomyces pombe*. J Cell Sci 75, 357–376.
Molliex A, Temirov J, Lee J, Coughlin M, Kanagaraj AP, Kim HJ, Mittag T, Taylor JP (2015). Phase separation by low complexity domains promotes stress granule assembly and drives pathological fibrillization. Cell 163, 123–133.
Monahan Z, Ryan VH, Janke AM, Burke KA, Rhoads SN, Zerze GH, O'Meally R, Dignon GL, Conicella AE, Zheng W, *et al*. (2017). Phosphorylation of the FUS low-complexity domain disrupts phase separation, aggregation, and toxicity. EMBO J 36, 2951–2967.
Moreno S, Klar A, Nurse P (1991). Molecular genetic analysis of fission yeast *Schizosaccharomyces pombe*. Methods Enzymol 194, 795–823.
Mutavchiev DR, Leda M, Sawin KE (2016). Remodeling of the fission yeast Cdc42 cell-polarity module via the Sty1 p38 stress-activated protein kinase pathway. Curr Biol, doi: 10.1016/j.cub.2016.08.048.
Nuñez I, Rodriguez Pino M, Wiley DJ, Das ME, Chen C, Goshima T, Kume K, Hirata D, Toda T, Verde F (2016). Spatial control of translation repression and polarized growth by conserved NDR kinase Orb6 and RNA-binding protein Sts5. eLife 5, doi: 10.7554/eLife.14216.
Nurse P, Bissett Y (1981). Gene required in G1 for commitment to cell cycle and in G2 for control of mitosis in fission yeast. Nature 292, 558–560.
Ocampo A, Barrientos A (2011). Quick and reliable assessment of chronological life span in yeast cell populations by flow cytometry. Mech Ageing Dev 132, 315–323.
Ohtsuka H, Ogawa S, Kawamura H, Sakai E, Ichinose K, Murakami H, Aiba H (2013). Screening for long-lived genes identifies Oga1, a guanine-quadruplex associated protein that affects the chronological lifespan of the fission yeast *Schizosaccharomyces pombe*. Mol Genet Genomics 288, 285–295.
Onken B, Wiener H, Philips MR, Chang EC (2006). Compartmentalized signaling of Ras in fission yeast. Proc Natl Acad Sci USA 103, 9045–9050.
Opalko HE, Moseley JB (2017). Dynamic regulation of Cdr1 kinase localization and phosphorylation during osmotic stress. J Biol Chem 292, 18457–18468.
Papadaki P, Pizon V, Onken B, Chang EC (2002). Two ras pathways in fission yeast are differentially regulated by two ras guanine nucleotide exchange factors. Mol Cell Biol 22, 4598–4606.
Perez-Hidalgo L, Moreno S (2016). Nutrients control cell size. Cell Cycle 15, 1655–1656.
Rabouille C, Alberti S (2017). Cell adaptation upon stress: the emerging role of membrane-less compartments. Curr Opin Cell Biol 47, 34–42.
Rallis C, Codlin S, Bahler J (2013). TORC1 signaling inhibition by rapamycin and caffeine affect lifespan, global gene expression, and cell proliferation of fission yeast. Aging Cell 12, 563–573.
Rauch N, Rukhlenko OS, Kolch W, Kholodenko BN (2016). MAPK kinase signalling dynamics regulate cell fate decisions and drug resistance. Curr Opin Struct Biol 41, 151–158.
Rauen KA (2013). The RASopathies. Annu Rev Genomics Hum Genet 14, 355–369.

Riback JA, Katanski CD, Kear-Scott JL, Pilipenko EV, Rojek AE, Sosnick TR, Drummond DA (2017). Stress-triggered phase separation is an adaptive, evolutionarily tuned response. Cell 168, 1028–1040.e1019.
Robinson SR, Oliver AW, Chevassut TJ, Newbury SF (2015). The 3′ to 5′ exoribonuclease DIS3: from structure and mechanisms to biological functions and role in human disease. Biomolecules 5, 1515–1539.
Ross DT, Scherf U, Eisen MB, Perou CM, Rees C, Spellman P, Iyer V, Jeffrey SS, Van de Rijn M, Waltham M, *et al.* (2000). Systematic variation in gene expression patterns in human cancer cell lines. Nat Genet 24, 227–235.
Roux AE, Leroux A, Alaamery MA, Hoffman CS, Chartrand P, Ferbeyre G, Rokeach LA (2009). Pro-aging effects of glucose signaling through a G protein-coupled glucose receptor in fission yeast. PLoS Genet 5, e1000408.
Roux AE, Quissac A, Chartrand P, Ferbeyre G, Rokeach LA (2006). Regulation of chronological aging in *Schizosaccharomyces pombe* by the protein kinases Pka1 and Sck2. Aging Cell 5, 345–357.
Schindelin J, Arganda-Carreras I, Frise E, Kaynig V, Longair M, Pietzsch T, Preibisch S, Rueden C, Saalfeld S, Schmid B, *et al.* (2012). Fiji: an open-source platform for biological-image analysis. Nat Methods 9, 676–682.
Sharif AAD, Hergovich A (2018). The NDR/LATS protein kinases in immunology and cancer biology. Semin Cancer Biol 48, 104–114.
Simanshu DK, Nissley DV, McCormick F (2017). RAS proteins and their regulators in human disease. Cell 170, 17–33.
Slack C, Alic N, Foley A, Cabecinha M, Hoddinott MP, Partridge L (2015). The Ras-Erk-ETS-signaling pathway is a drug target for longevity. Cell 162, 72–83.
Stegert MR, Hergovich A, Tamaskovic R, Bichsel SJ, Hemmings BA (2005). Regulation of NDR protein kinase by hydrophobic motif phosphorylation mediated by the mammalian Ste20-like kinase MST3. Mol Cell Biol 25, 11019–11029.
Su SS, Tanaka Y, Samejima I, Tanaka K, Yanagida M (1996). A nitrogen starvation-induced dormant G0 state in fission yeast: the establishment from uncommitted G1 state and its delay for return to proliferation. J Cell Sci 109 (Pt 6), 1347–1357.
Swaffer MP, Jones AW, Flynn HR, Snijders AP, Nurse P (2018). Quantitative phosphoproteomics reveals the signaling dynamics of cell-cycle kinases in the fission yeast *Schizosaccharomyces pombe*. Cell Rep 24, 503–514.
Tatebe H, Nakano K, Maximo R, Shiozaki K (2008). Pom1 DYRK regulates localization of the Rga4 GAP to ensure bipolar activation of Cdc42 in fission yeast. Curr Biol 18, 322–330.
Tay YD, Leda M, Spanos C, Rappsilber J, Goryachev AB, Sawin KE (2019). Fission yeast NDR/LATS kinase Orb6 regulates exocytosis via phosphorylation of the exocyst complex. Cell Rep 26, 1654–1667.e1657.
Tidyman WE, Rauen KA (2016). Expansion of the RASopathies. Curr Genet Med Rep 4, 57–64.
Toda T, Niwa H, Nemoto T, Dhut S, Eddison M, Matsusaka T, Yanagida M, Hirata D (1996). The fission yeast sts5+ gene is required for maintenance of growth polarity and functionally interacts with protein kinase C and an osmosensing MAP-kinase pathway. J Cell Sci 109 (Pt 9), 2331–2342.
Tratner I, Fourticq-Esqueoute A, Tillit J, Baldacci G (1997). Cloning and characterization of the *S. pombe* gene efc25+, a new putative guanine nucleotide exchange factor. Gene 193, 203–210.
Verde F, Mata J, Nurse P (1995). Fission yeast cell morphogenesis: identification of new genes and analysis of their role during the cell cycle. J Cell Biol 131, 1529–1538.
Verde F, Wiley DJ, Nurse P (1998). Fission yeast orb6, a ser/thr protein kinase related to mammalian rho kinase and myotonic dystrophy kinase, is required for maintenance of cell polarity and coordinates cell morphogenesis with the cell cycle. Proc Natl Acad Sci USA 95, 7526–7531.
Vjestica A, Zhang D, Liu J, Oliferenko S (2013). Hsp70-Hsp40 chaperone complex functions in controlling polarized growth by repressing Hsf1-driven heat stress-associated transcription. PLoS Genet 9, e1003886.
Wanless AG, Lin Y, Weiss EL (2014). Cell morphogenesis proteins are translationally controlled through UTRs by the Ndr/LATS target Ssd1. PLoS One 9, e85212.
Wei M, Fabrizio P, Hu J, Ge H, Cheng C, Li L, Longo VD (2008). Life span extension by calorie restriction depends on Rim15 and transcription factors downstream of Ras/PKA, Tor, and Sch9. PLoS Genet 4, e13.
Wiley DJ, Marcus S, D'Urso G, Verde F (2003). Control of cell polarity in fission yeast by association of Orb6p kinase with the highly conserved protein methyltransferase Skb1p. J Biol Chem 278, 25256–25263.
Yaffe MB, Rittinger K, Volinia S, Caron PR, Aitken A, Leffers H, Gamblin SJ, Smerdon SJ, Cantley LC (1997). The structural basis for 14-3-3:phosphopeptide binding specificity. Cell 91, 961–971.
Yanagida M (2009). Cellular quiescence: are controlling genes conserved? Trends Cell Biol 19, 705–715.
Yanagida M, Ikai N, Shimanuki M, Sajiki K (2011). Nutrient limitations alter cell division control and chromosome segregation through growth-related kinases and phosphatases. Philos Trans R Soc Lond B Biol Sci 366, 3508–3520.
Zhang L, Tang F, Terracciano L, Hynx D, Kohler R, Bichet S, Hess D, Cron P, Hemmings BA, Hergovich A, *et al.* (2015). NDR functions as a physiological YAP1 kinase in the intestinal epithelium. Curr Biol 25, 296–305.
Zinn K (2004). Dendritic tiling: new insights from genetics. Neuron 44, 211–213.
Zuin A, Carmona M, Morales-Ivorra I, Gabrielli N, Vivancos AP, Ayte J, Hidalgo E (2010). Lifespan extension by calorie restriction relies on the Sty1 MAP kinase stress pathway. EMBO J 29, 981–991.